Poisson multi-Bernoulli mixture filter for trajectory measurements

Marco Fontana, Ángel F. García-Fernández, Simon Maskell

***Abstract*—This paper presents a Poisson multi-Bernoulli mixture (PMBM) filter for multi-target filtering based on sensor measurements that are sets of trajectories in the last two-time step window. The proposed filter, the trajectory measurement PMBM (TM-PMBM) filter, propagates a PMBM density on the set of target states. In prediction, the filter obtains the PMBM density on the set of trajectories over the last two time steps. This density is then updated with the set of trajectory measurements. After the update step, the PMBM posterior on the set of two-step trajectories is marginalised to obtain a PMBM density on the set of target states. The filter provides a closed-form solution for multi-target filtering based on sets of trajectory measurements, estimating the set of target states at the end of each time window. Additionally, the paper proposes computationally lighter alternatives to the TM-PMBM filter by deriving a Poisson multi-Bernoulli (PMB) density through Kullback-Leibler divergence minimisation in an augmented space with auxiliary variables. The performance of the proposed filters are evaluated in a simulation study.**

***Index Terms*—Bayesian estimation, multi-target filtering, Poisson multi-Bernoulli mixture filter, trajectory measurements.**

I. Introduction

Multi-target filtering is the algorithmic process of continuously estimating a time-evolving set of target states in a stochastic environment, based on incoming noisy data streams [1]–[3]. It has widespread applications, including radar and sonar tracking, autonomous vehicle navigation, video surveillance, and biological studies [4]–[7].

Some of the most widely used approaches include multiple hypothesis tracking (MHT) [8], joint probabilistic data association (JPDA) [9], and random finite sets (RFS) [10]. Finite Set Statistics (FISST) can be used to provide a general Bayesian framework for multi-target filtering problems involving an unknown and time-varying number of targets [11], [12]. This approach models both multi-target states and multi-target measurements as RFSs under a rigorous unified framework [10], which is closely related to point process theory [13]. An early approximate solution to the multi-target filtering problem based on FISST is the Probability Hypothesis Density (PHD) filter [14]. More recently, RFS-based filters that generate explicit data association hypotheses have been introduced, such as the Poisson multi-Bernoulli mixture (PMBM) filter [15], the multi-Bernoulli mixture (MBM) filter [15], [16] and the generalised labelled multi-Bernoulli (GLMB) [17]. Finally, in recent years, methods aimed at estimating sets of target trajectories directly from the posterior density on the set of trajectories have been proposed [18], [19].

Standard multi-target filtering algorithms are typically designed for detectors that provide information on the set of targets at specific, discrete points in time. The standard point-target measurement model [20, Sec. 12.3], as well as the extended target [21] and track-before-detect [22] measurement models commonly found in the literature are based on this assumption. Nevertheless, certain sensors may generate measurements that span a time interval during which the target may have moved.

For instance, the detector for distributed acoustic sensing proposed in [23] operates within a time window producing detections that are trajectories. Each of these trajectory measurements may have been generated by a target or by clutter. Trajectory measurements can also be generated by some track-before-detect (TkBD) processing methods, which delay target declaration until enough data has been accumulated [24]. Various batch processing algorithms, such as envelope interpolation, maximum likelihood estimation [25], and dynamic programming [26], also follow this approach. When integration periods are extended with minimal acceleration, individual scans form straight lines in Cartesian-time or range-Doppler frequency-time space [27], detectable using techniques like the Hough transform [28], [29], RANSAC [30], and Expectation-Maximization [31]. Each line can be characterised by estimating the initial position and velocity of the target [32].

In space surveillance, fast-moving satellites may appear as streaks (trajectory measurements) in telescope images, particularly in low SNR conditions [33], [34]. A method for tracking streaking targets in video frames using the Maximum Likelihood Probabilistic Multi-Hypothesis Tracker (MLPMHT) [35] and a target state defined by the starting and ending positions in each batch was proposed in [34].

Trajectory measurements may also arise in a multi-sensor scenario, where multiple measurements, presumably for the same target, are combined at the sensor level of a 'composite measurement fusion' architecture [36]. These trajectory measurements, or the tracklets derived from them [1, Ch. 10], are subsequently used to update the global tracks, which are maintained at the central level of the system.

Motivated by the need for multi-target filters capable of processing trajectory measurements, we develop a multi-target PMBM filter, referred to as trajectory measurement PMBM

M. Fontana and S. Maskell are with the Department of Electrical Engineering and Electronics, University of Liverpool, Liverpool L69 3GJ, United Kingdom (emails: {marco.fontana, s.maskell}@liverpool.ac.uk).
Á. F. García-Fernández was with the Department of Electrical Engineering and Electronics, University of Liverpool, Liverpool L69 3GJ, United Kingdom. He is now with the IPTC, ETSI de Telecomunicación, Universidad Politécnica de Madrid, Av. Complutense 30, 28040, Madrid, Spain (e-mail: angel.garcia.fernandez@upm.es).

(TM-PMBM), that provides the closed-form recursion for computing the posterior distribution of the set of targets given a sequence of sets of trajectory measurements, each lasting up to two time steps. These measurement trajectories can represent point detections at time steps k and $k+1$, and also straight lines between time steps k and $k+1$, as illustrated in Fig. 1. In this paper, each measurement of this type is a trajectory that can last up to two time steps, and is referred to as trajectory measurement. The set of received measurements at each time step is therefore a set of trajectories [19], comprising both target-generated trajectory measurements and clutter trajectory measurements. Note that, whereas existing trajectory PMBM filters [18], [19], [37] estimate trajectories from point measurements, the proposed filter derives a closed-form PMBM recursion that directly processes raw two-time step trajectory observations obtained at the sensor level.

Fig. 2 shows a schematic of the proposed filter. At each time window, spanning from time step k to $k+1$, the prediction step is applied to the posterior PMBM density on the set of target states at time step k, resulting in a PMBM density according to the trajectory PMBM filter prediction step [37]. The resulting predicted PMBM density is defined over two-step trajectories which, like the trajectory measurements, consist of up to two target states: one at time step k and one at $k+1$. Since each trajectory measurement in the current time window can contain information on a target trajectory from time step k to $k+1$, the update step in this interval must be applied on the density that contains information on the target trajectories from time step k to $k+1$, resulting in the posterior PMBM density over the two-step trajectories. Finally, the marginalisation step retains only the information on the set of targets at time step $k+1$, resulting in the PMBM posterior density on the target states. This paper also proposes the Gaussian implementation of the TM-PMBM filter, which is trajectory-measurement version of the (track-oriented) PMB filter in [38] and can be derived via KLD minimisation with auxiliary variables [39].

The remainder of the paper is organised as follows. In Section II, we outline the multitarget filtering problem by defining the variables and models for trajectory measurements and two-step (target) trajectories. In Section III, we derive the TM-PMBM filtering recursion, outlining the prediction, update and marginalisation steps. The Gaussian implementation of the proposed TM-PMBM filter is presented in Section IV, while Section IV-E describes the TM-PMB filter. Finally, Section V presents the simulation results, followed by the conclusions drawn in Section VI.

II. Problem Formulation

We develop the multi-target PMBM filter where, at each time step, the set of measurements contains trajectories in the last two time steps. Similarly to the point-target measurement model [10], each target can generate at most one target-generated trajectory measurement. The set of trajectory measurements also contains clutter. To introduce this problem, we first explain the required variables and notation involved.

In Section II-A, we define the notation used to represent target states, two-step (target) trajectories and trajectory measurements, along with their corresponding spaces. Section II-B

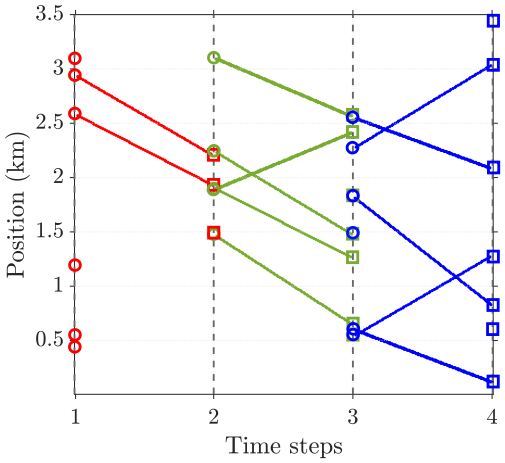

Figure 1: An example of three sets of trajectory measurements across three time windows, spanning time steps 1 to 4. Each set of trajectory measurements is represented by a distinct colour. The vertical dashed lines indicate the start and end of each time window. Each trajectory measurement is either a trajectory connecting two one-dimensional point detections at time step k (circle) and $k+1$ (square), a point detection at time step k or a point detection at time step $k+1$.

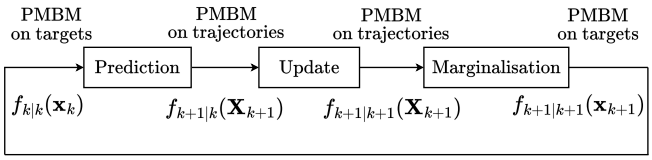

Figure 2: Diagram of the PMBM filter based on trajectory measurements, the TM-PMBM filter. After the prediction from time step k, the TM-PMBM filter incorporates information on the set of trajectories at time steps k and $k+1$, resulting in a PMBM density on this set of trajectories. The trajectory measurements at time step $k+1$, which can span the time steps k and $k+1$, are then used to update the PMBM density on the set of trajectories at time steps k and $k+1$. A marginalisation step is then done to keep the information on the set of targets at time step $k+1$. This step also results in PMBM density.

reviews the standard transition model and the PPP birth model, extending them to the context of the two-step trajectories. Section II-C introduces the measurement model we propose for two-step trajectories. Finally, Section II-D revisits the PMBM posterior density over the set of targets and extends it to the set of two-step trajectories.

A. Variables

1) Single-target state and set of targets: In the context of multi-target systems, we regard filtering as the estimation of the states of a time-varying number of targets at the current time step $k \in \mathbb{N}^+$. We denote a single-target state as $x_k \in \mathbb{R}^{n_x}$, and the set of target states at time k as $\mathbf{x}_k \in \mathcal{F}(\mathbb{R}^{n_x})$, where $\mathcal{F}(\mathbb{R}^{n_x})$ is the set of all finite subsets of $\mathbb{R}^{n_x}$. The set $\mathbf{x}_k$ is modelled as a random finite set, meaning that both the cardinality $|\mathbf{x}_k|$ and the elements of the set (i.e., the target states) are random variables [10].

2) Single-trajectory state and set of trajectories over k and $k+1$: We consider that the time window $k+1$ is defined by two consecutive time steps k and $k+1$. The space of the

single target trajectories in this time window, is denoted by $T_{(k+1)}$. That is, $T_{(k+1)}$ is the disjoint union of three distinct spaces. These spaces represent the following cases: there is a single target present at time step k but not at time step $k+1$, there is a single target born at time step $k+1$, and there is a single target present at both time steps k and $k+1$. That is, mathematically, we can write the single-trajectory space for time steps k and $k+1$ as [19]

$$\begin{aligned} T_{(k+1)} &= T^1_{(k+1)} \uplus T^2_{(k+1)} \uplus T^3_{(k+1)} \\ &= \left[\{k\} \times \mathbb{R}^{n_x}\right] \uplus \left[\{k+1\} \times \mathbb{R}^{n_x}\right] \uplus \left[\{k\} \times \mathbb{R}^{2n_x}\right], \end{aligned} \tag{1}$$

where $\uplus$ stands for disjoint union. Given a trajectory $(t, x_{1:\nu}) \in T_{(k+1)}$, t represents the initial time step of the single trajectory (which is either k or $k+1$), and $x_{1:\nu} = (x_1, ..., x_\nu)$ represents the sequence of target states, with ν being the length of the trajectory.

More specifically, a two-step trajectory $X_{k+1} \in T_{(k+1)}$ has the form

$$X_{k+1} = \begin{cases} (k, x_1) & X_{k+1} \in T^1_{(k+1)} \quad (2a) \\ (k+1, x_1) & X_{k+1} \in T^2_{(k+1)} \quad (2b) \\ (k, x_{1:2}) & X_{k+1} \in T^3_{(k+1)}. \quad (2c) \end{cases}$$

Line (2a) indicates a trajectory that died in the time window, i.e., it exists at time step k, but it does not at time step $k+1$. Line (2b) indicates a trajectory that was born at time step $k+1$. Line (2c) indicates a trajectory that exists at time step k and $k+1$ (with two states x_1 and x_2, $x_{1:2} \in \mathbb{R}^{2n_x}$).

A set of two-step trajectories is denoted by $\mathbf{X}_{k+1} \in \mathcal{F}\left(T_{(k+1)}\right)$, where $\mathcal{F}\left(T_{(k+1)}\right)$ denotes the set of all finite subsets of $T_{(k+1)}$. All mathematical formalities on sets of trajectories can be found in [19].

3) Single-trajectory measurement and set of trajectory measurements over k and $k+1$: We denote a single n_z-dimensional measurement as $z \in \mathbb{R}^{n_z}$, and the set of measurements at time k as $\mathbf{z}_k \in \mathcal{F}(\mathbb{R}^{n_z})$. Analogously to (1), we define the space of trajectory measurements $M_{(k+1)}$ in the time window from k to $k+1$ as the disjoint union of three spaces: measurement space with a detection at time step k but not at time step $k+1$, measurement space with a detection only at time step $k+1$, and measurement space with a detection at both time steps k and $k+1$. That is, mathematically, we can write

$$\begin{aligned} M_{(k+1)} &= M^1_{(k+1)} \uplus M^2_{(k+1)} \uplus M^3_{(k+1)} \\ &= \left[\{k\} \times \mathbb{R}^{n_z}\right] \uplus \left[\{k+1\} \times \mathbb{R}^{n_z}\right] \uplus \left[\{k\} \times \mathbb{R}^{2n_z}\right]. \end{aligned} \tag{3}$$

Given a trajectory measurement $(t, z_{1:m}) \in M_{(k+1)}$, t represents the initial time step of the trajectory measurement, and $z_{1:\iota} = (z_1, ..., z_\iota)$ represents the sequence of ι measurements.

Therefore, a trajectory measurement Z_{k+1} in the interval from k and to $k+1$ has the form

$$Z_{k+1} = \begin{cases} (k, z_1) & Z_{k+1} \in M^1_{(k+1)} \quad (4a) \\ (k+1, z_1) & Z_{k+1} \in M^2_{(k+1)} \quad (4b) \\ (k, z_{1:2}) & Z_{k+1} \in M^3_{(k+1)}, \quad (4c) \end{cases}$$

where $z_1 \in \mathbb{R}^{n_z}$ is an n_z-dimensional measurement, and $z_{1:2}$ expresses the measurement at both time steps. We call a trajectory measurement a full (trajectory) measurement if it contains two measurements at two time steps. On the other hand, the trajectory measurement is defined as partial if it only contains a measurement at one time step. A set of trajectory measurements is denoted by $\mathbf{Z}_{k+1} \in \mathcal{F}\left(M_{(k+1)}\right)$.

4) Trajectory integrals: Given a trajectory at the current time window $X_{k+1} = (t, x_{1:\nu}) \in T_{(k+1)}$, the variable (t, ν) belongs to the set $I_{(k:k+1)} = \{(t, \nu) : t \in \{k, k+1\} \text{ and } 1 \leq \nu \leq k - t + 1\}$. The integral of a real-valued function $\pi(\cdot)$ on the single-trajectory space $T_{(k+1)}$ is [19]

$$\begin{aligned} \int \pi(X)\, dX &= \sum_{(t,\nu) \in I_{(k:k+1)}} \int \pi(t, x_{1:\nu})\, dx_{1:\nu} \\ &= \int \pi(k, x_{1:2})\, dx_{1:2} + \int \pi(k, x_1)\, dx_1 \\ &\quad + \int \pi(k+1, x_1)\, dx_1. \end{aligned} \tag{5}$$

This integral spans across all potential start times, durations, and states of the two-step trajectory.

Given a real-valued function $\pi(\cdot)$ on the space $\mathcal{F}\left(T_{(k+1)}\right)$ of sets of two-step trajectories, its set integral is

$$\int \pi(\mathbf{X})\, \delta\mathbf{X} = \sum_{n=0}^{\infty} \frac{1}{n!} \int \pi(\{X_1, ..., X_n\})\, dX_{1:n}, \tag{6}$$

where $X_{1:n} = (X_1, \ldots, X_n)$.

B. Dynamic model

We consider the standard dynamic model for sets of targets [10]. That is, given a set of targets $\mathbf{x}_k$, each target $x_k \in \mathbf{x}_k$ at time step k survives to the time step $k+1$ with a probability of survival $p^S(x_k)$, according to a Markov transition density $g(x_{k+1}|x_k)$. Alternatively, the target dies with probability $1 - p^S(x_k)$. At each time step, targets are born independently of existing targets according to a PPP with intensity $\lambda^B_k(x_k)$. Given this transition model for sets of targets, we can write it in terms of the trajectories.

1) Transition model for trajectories in k and $k+1$: This section explains the transition model of the set of targets at time k when we keep the trajectory information of the target at time steps k and $k+1$. We keep the information on all trajectories [37], as this will be required for the update step.

Given the set of target states $\mathbf{x}_k$ at time step k, each target state $x \in \mathbf{x}_k$ evolves with probability 1 into a trajectory $Y = (t, y_{1:\nu})$, defined between time steps k and $k+1$. In this case, the transition density is [37]

$$g_{k+1}(Y|x) = \begin{cases} \delta_k[t]\delta_x(y_1)p^S(x)g(y_2|x) & Y = (k, y_{1:2}) \quad (7a) \\ \delta_k[t]\delta_x(y_1)\left(1 - p^S(x)\right) & Y = (k, y_1) \quad (7b) \\ 0 & \text{otherwise.} \quad (7c) \end{cases}$$

where $\delta_k[\cdot]$ is a Kronecker delta located at k, and $\delta_x(\cdot)$ is a Dirac delta located at x. Line (7a) corresponds to the case where the trajectory is present at time steps k and $k+1$, while in (7b) the trajectory is only present at time step k.

Note that the probability that each target at time step k is kept in the set of trajectories from time step k and $k+1$ is one, as this set includes all trajectories at time steps k and $k+1$. This also happens in the dynamic model for tracking the set of all trajectories if we keep information on the set of all trajectories up to the current time step [40].

2) Birth model: The multi-trajectory state $\mathbf{X}_{k+1}$ is the union of the surviving trajectories and new born trajectories. As explained before, new targets are born independently at each time step following a PPP with intensity $\lambda^B_{k+1}(\cdot)$. This implies that the intensity for new born trajectories is [39]

$$\lambda^B_{k+1}(X) = \begin{cases} \lambda^B_{k+1}(x_1) & X = (k+1, x_1) \\ 0 & \text{otherwise.} \end{cases} \tag{8}$$

C. Trajectory-measurement model

This section explains the model of the trajectory measurements we consider. Each two-step trajectory $X \in T^{\tau}_{(k+1)}$, $\tau \in \{1,2,3\}$, is detected with probability $p^D(X_{k+1})$ and generates one trajectory measurement $Z \in M^{\mu}_{(k+1)}$, $\mu \in \{1,2,3\}$, with density

$$l\left(Z|X\right) = \begin{cases} \gamma h_{1,3}(z_1|x_{1:2}) & Z=(k,z_1), X=(k,x_{1:2}) & \text{(9a)} \\ \gamma h_{2,3}(z_1|x_{1:2}) & Z=(k+1,z_1), X=(k,x_{1:2}) & \text{(9b)} \\ \widetilde{p}^D h_{3,3}(z_{1:2}|x_{1:2}) & Z=(k,z_{1:2}), X=(k,x_{1:2}) & \text{(9c)} \\ h_{1,1}(z_1|x_1) & Z=(k,z_1), X=(k,x_1) & \text{(9d)} \\ h_{2,2}(z_1|x_1) & Z=(k+1,z_1), X=(k+1,x_1) & \text{(9e)} \\ 0 & \text{otherwise,} & \text{(9f)} \end{cases}$$

where $\widetilde{p}^D$ is the probability of receiving a full trajectory measurement conditioned on the existence of a trajectory $X = (k, x_{1:2})$, and $h_{\mu,\tau}(\cdot|\cdot)$ are densities on the single-trajectory measurement space, conditioned on the target state. Finally, we set $\gamma = 0.5\left(1-\widetilde{p}^D\right)$ such that the integral of $l(Z|X)$ (over the single-trajectory space), given $X=(k,x_{1:2})$, is unity and the detection of either end of the trajectory has equal probability. Alternatively, the trajectory is not detected with probability $1-p^D(X)$.

Clutter is distributed according to a PPP with intensity $\lambda^C(\cdot)$ on the trajectory-measurement space. More information on PPPs for sets of trajectories can be found in [18].

D. PMBM posterior and predicted densities

Given the dynamic and measurement models, our objective is to compute the posterior density $f_{k+1|k+1}(\cdot)$ over the set of targets given the sequence of trajectory measurements up to the time step $k+1$. For these models, both the posterior and predicted densities are PMBMs [37], [39]. We proceed to give an overview of the PMBM posterior and predicted densities for both targets and trajectories.

1) PMBM density on targets: The PMBM posterior and predicted densities over the set of target states $\mathbf{x}_{k'}$ at time step k', with $k' \in \{k, k+1\}$, are expressed as [15]

$$f_{k+1|k'}\left(\mathbf{x}_{k'}\right) = \sum_{\uplus_{l=1}^{n_{k+1|k'}} \mathbf{x}^l \uplus \mathbf{y} = \mathbf{x}_{k'}} f^p_{k+1|k'}\left(\mathbf{y}\right) f^{mbm}_{k+1|k}(\mathbf{x}), \tag{10}$$

where the sum goes over all mutually disjoint sets $\mathbf{y}$ and $\mathbf{x}$, such that their union is $\mathbf{x}_{k'}$. The two densities in (10) are explained next.

The PPP density represents the targets that exist at the current time instant, but have not yet been detected. Its density is

$$f^p_{k+1|k'}(\mathbf{x}) = e^{-\int \lambda_{k+1|k'}(x)dx} \prod_{x\in\mathbf{x}} \lambda_{k+1|k'}(x), \tag{11}$$

where $\lambda_{k+1|k'}(\cdot)$ is the intensity. In the PPP, the cardinality is Poisson distributed and targets are independent, and identically distributed. The MBM part represents the potential targets that have been detected at some point up to the current time step, and it can be described as [38]:

$$f^{mbm}_{k+1|k'}(\mathbf{x}) = \sum_{a\in\mathcal{A}_{k+1|k'}} w^a_{k+1|k'} \sum_{\uplus_{j=1}^{n_{k+1|k'}} \mathbf{x}^j = \mathbf{x}} \prod_{i=1}^{n_{k+1|k'}} f^{i,a^i}_{k+1|k'}(\mathbf{x}^i), \tag{12}$$

where i is the index over the Bernoulli components, $a = (a^1, \ldots, a^{n_{k+1|k'}})$ represents a specific global data association hypothesis, $a^i \in \{1, \ldots, h^i_{k+1|k'}\}$ is an index over the $h^i_{k+1|k'}$ single target hypotheses for the i-th potential target, $\mathcal{A}_{k+1|k'}$ is the set of global hypotheses, and $n_{k+1|k'}$ is the number of potentially detected targets. Each global hypothesis is associated to a weight $w^a_{k+1|k'}$ satisfying $\sum_{a\in\mathcal{A}_{k+1|k'}} w^a_{k+1|k'} = 1$. The Bernoulli density corresponding to the i-th potential target, $i \in \{1, \ldots n_{k+1|k'}\}$ and the a_i single target hypothesis density $f^{i,a^i}_{k+1|k'}(\cdot)$ can be expressed as

$$f^{i,a^i}_{k+1|k'}\left(\mathbf{x}\right) = \begin{cases} 1 - r^{i,a^i}_{k+1|k'} & \mathbf{x} = \emptyset & \text{(13a)} \\ r^{i,a^i}_{k+1|k'} p^{i,a^i}_{k+1|k'}(x) & \mathbf{x} = \{x\} & \text{(13b)} \\ 0 & \text{otherwise,} & \text{(13c)} \end{cases}$$

where $r^{i,a^i}_{k+1|k'} \in [0,1]$ is the probability of existence and $p^{i,a^i}_{k+1|k'}(\cdot)$ is the single-target density given that it exists.

2) PMBM on sets of trajectories from k to $k+1$: Following [37], [39], we extend the PMBM filtering/predicted density over the set of two-step trajectories. Given a PMBM density on the set of target states at the time step k of the form (10), the transition and measurement models for trajectories indicated in Sections II-B1 and II-C, the predicted and updated densities on the set of two-step trajectories $\mathbf{X}_{k+1}$ from time step k to $k+1$ are also PMBMs of the form

$$f_{k+1|k'}\left(\mathbf{X}_{k'}\right) = \sum_{\uplus_{l=1}^{n_{k+1|k'}} \mathbf{X}^l \uplus \mathbf{Y} = \mathbf{X}_{k'}} f^p_{k+1|k'}\left(\mathbf{Y}\right) f^{mbm}_{k+1|k'}(\mathbf{X}), \tag{14}$$

where $n_{k+1|k} = n_{k|k}$ and $f^p_{k+1|k'}(\cdot)$ and $f^{mbm}_{k+1|k'}(\cdot)$ are the PPP and MBM densities for the two-time step trajectories. This result is obtained as a consequence of the prediction and update steps of the trajectory PMBM filter (PMBM filter on the sets of trajectories) [41]. It should be noted that when we receive trajectory measurements, the local and global hypotheses are defined as for standard measurements, with the only difference that standard point target measurements are now two-step trajectories. To continue with the PMBM

filtering recursion on the set of targets, the density (14) is then marginalised to obtain a density of the form (10) on the target states $\mathbf{x}_{k+1}$ at time $k+1$.

III. TM-PMBM FILTERING RECURSION

This section presents the filtering recursion of the TM-PMBM filter, whose diagram is provided in Fig. 2. At each time step k, the PMBM density on the set of targets $\mathbf{x}_k$ is of the form (10). In Section III-A, we perform the prediction step based on the transition density (7) to obtain the predicted PMBM density (14) on the set of two-step trajectories $\mathbf{X}_{k+1}$ in the time window $k+1$, defined by the time steps k and $k+1$. In Section III-B, we update the density on two-step trajectories based on the set of trajectory measurements $\mathbf{Z}_{k+1}$ in the time window $k+1$. In Section III-C, the density (14) is then marginalised to obtain a density of the form (10) on the target states $\mathbf{x}_{k+1}$ at time $k+1$.

In this section, we use the following notation. Given two real-valued functions $a(\cdot)$ and $b(\cdot)$ on either the single-target space or the single-trajectory space, their inner product is denoted by [39], [42]

$$\langle a, b \rangle = \int a(X) b(X)\, dX. \tag{15}$$

A. Prediction

The predicted PMBM density over the set of two-step trajectories is derived from the posterior PMBM density after the marginalisation described in Section III-C. For clarity, we use the superscript M to denote densities and parameters that define the marginalised posterior at time step k.

With the transition model in (7), and applying the prediction step of the TPMBM filter for the set of all trajectories [41], the predicted PMBM density is of the form (14) with $n_{k+1|k} = n_{k|k}$.

Lemma 1 (TM-PMBM prediction)**.** *Given the PMBM filtering density on the set of target states at time step k of the form (10), the predicted density at time $k+1$ is a PMBM of the form (14), with $n_{k+1|k} = n_{k|k}$ and Poisson intensity*

$$\lambda_{k+1|k}(X_{k+1}) = \lambda^B_{k+1}(X_{k+1}) + \left\langle \lambda^M_{k|k}, g_{k+1}(X_{k+1}|\cdot) \right\rangle. \tag{16}$$

Each Bernoulli component $f^{i,a^i}_{k+1|k}(\cdot)$, $i \in \{1, \ldots, n_{k+1|k}\}$, $a^i \in \{1, \ldots, h^i_{k+1|k}\}$, in the MBM part is defined by

$$r^{i,a^i}_{k+1|k} = r^{i,a^i,M}_{k|k} \tag{17}$$

$$p^{i,a^i}_{k+1|k}(X_{k+1}) = \left\langle p^{i,a^i,M}_{k|k}, g_{k+1}(X_{k+1}|\cdot) \right\rangle. \tag{18}$$

B. Update

Given the trajectory measurement model in Section II-C, the TM-PMBM filter update is provided in the following lemma.

Lemma 2 (TM-PMBM update)**.** *Given a set of trajectory measurements $\mathbf{Z}_{k+1} = \{Z^1_{k+1}, \ldots, Z^{m_{k+1}}_{k+1}\}$ in the time window between time steps k and $k+1$, and a PMBM predicted density on the set of two-step trajectories of the form (14), the updated distribution is exactly a PMBM density of the form (14) with $n_{k+1|k+1} = n_{k+1|k} + m_{k+1}$ and Poisson intensity*

$$\lambda_{k+1|k+1}(X) = \left(1 - p^D(X)\right) \lambda_{k+1|k}(X). \tag{19}$$

For each Bernoulli component in $f^{i,a^i}_{k+1|k}(\cdot)$, $i \in \{1, \ldots, n_{k+1|k}\}$, $a^i \in \{1, \ldots, h^i_{k+1|k}\}$, there is a missed detection hypothesis with the following parameters

$$w^{i,a^i}_{k+1|k+1} = 1 - r^{i,a^i}_{k+1|k} \left\langle p^{i,a^i}_{k+1|k}, p^D \right\rangle \tag{20}$$

$$r^{i,a^i}_{k+1|k+1} = \frac{r^{i,a^i}_{k+1|k} \left\langle p^{i,a^i}_{k+1|k}, 1 - p^D \right\rangle}{1 - r^{i,a^i}_{k+1|k} \left\langle p^{i,a^i}_{k+1|k}, p^D \right\rangle} \tag{21}$$

$$p^{i,a^i}_{k+1|k+1}(X) = \frac{\left(1 - p^D(X)\right) p^{i,a^i}_{k+1|k}(X)}{\left\langle p^{i,a^i}_{k+1|k}, 1 - p^D \right\rangle}. \tag{22}$$

The hypothesis for the existing Bernoulli component $f^{i,\widetilde{a}^i}_{k+1|k}(\cdot)$, $i \in \{1, \ldots, n_{k+1|k}\}$, $\widetilde{a}^i \in \{1, \ldots, h^i_{k+1|k}\}$, and trajectory measurement Z^j_{k+1} has index $a^i = \widetilde{a}^i + h^i_{k+1|k}$ and parameters

$$r^{i,a^i}_{k+1|k+1} = 1 \tag{23}$$

$$w^{i,a^i}_{k+1|k+1} = r^{i,\widetilde{a}^i}_{k+1|k} \left\langle p^{i,\widetilde{a}^i}_{k+1|k}, l\left(Z^j_{k+1}|\cdot\right) p^D \right\rangle \tag{24}$$

$$p^{i,a^i}_{k+1|k+1}(X) = \frac{l\left(Z^j_{k+1}|X\right) p^D(X) p^{i,\widetilde{a}^i}_{k+1|k}(X)}{\left\langle p^{i,\widetilde{a}^i}_{k+1|k}, l\left(Z^j_{k+1}|\cdot\right) p^D(\cdot) \right\rangle}. \tag{25}$$

For a new Bernoulli component $i = n_{k+1|k} + j$, $j \in \{1, \ldots, m_{k+1}\}$, initiated by the trajectory measurement Z^j_{k+1}, there are two local hypotheses: missed detection with parameters $w^{i,1}_{k+1|k+1} = 1$, $r_{k+1|k+1} = 0$, and detection with parameters

$$w^{i,2}_{k+1|k+1} = \lambda^C(Z^j_{k+1}) + \left\langle \lambda_{k+1|k}, l\left(Z^j_{k+1}|\cdot\right) p^D(\cdot) \right\rangle \tag{26}$$

$$r^{i,2}_{k+1|k+1} = \frac{\left\langle \lambda_{k+1|k}, l\left(Z^j_{k+1}|\cdot\right) p^D(\cdot) \right\rangle}{\lambda^C(Z^j_{k+1}) + \left\langle \lambda_{k+1|k}, l\left(Z^j_{k+1}|\cdot\right) p^D(\cdot) \right\rangle} \tag{27}$$

$$p^{i,2}_{k+1|k+1}(X) = \frac{l\left(Z^j_{k+1}|X\right) p^D(X) \lambda_{k+1|k}(X)}{\left\langle \lambda_{k+1|k}, l\left(Z^j_{k+1}|\cdot\right) p^D(\cdot) \right\rangle}. \tag{28}$$

This update is a direct result of the update steps of the PMBM filter [38] and the TPMBM filter for point targets [37]. It should be noted that the TM-PMBM update step is applied on the density on the sets of trajectories between time steps k and $k+1$ because the trajectory measurements contain information on the trajectories on these two time steps. This is also required to compute the dot products in this lemma.

C. Marginalisation

In this paper, once we have performed the update in Lemma 2, we are only interested in keeping the information on the set of targets at the end of the time window, i.e., at time step

$k+1$. To do so, we perform a marginalisation step after we have performed the update, integrating out the trajectory states at time step k while retaining the information corresponding to time step $k+1$. The marginalisation theorem for general densities on sets of trajectories is provided in Theorem 11 in [19]. The marginalisation theorem applied to PMBMs on sets of trajectories is provided in [37]. The result is another PMBM on the set of targets at time step $k+1$.

The marginalisation step can be carried out in an exact manner by choosing a suitable multi-target transition model (distinct from the one used in the prediction step) and performing a PMBM prediction step. We proceed to explain the multi-target transition model to perform the marginalisation, which includes a probability of survival and a single-target transition density.

We consider a two-step trajectory $X_{k+1} = (t, x_{1:\nu}) \in T_{(k+1)}$. The probability of survival at the marginalisation stage is

$$p_{k+1}^{S,M}(X_{k+1}) = \begin{cases} 0 & X_{k+1} \in T_{(k+1)}^1 \quad (29a) \\ 1 & X_{k+1} \in T_{(k+1)}^2 \quad (29b) \\ 1 & X_{k+1} \in T_{(k+1)}^3. \quad (29c) \end{cases}$$

That is, two-step trajectories that belong to $T_{(k+1)}^1$, are those that do not exist at time step k so they are not included in the set of targets at time step $k+1$. On the contrary, two-step trajectories that belong to $T_{(k+1)}^2$ and $T_{(k+1)}^3$ have a target state at time step $k+1$ so their probability of survival is one. Then, we apply the single-target transition density to each surviving target

$$g_{k+1}^M(x_{k+1}|X) = \begin{cases} \delta_{x_2}(x_{k+1}) & X = (k, x_{1:2}) \quad (30a) \\ \delta_{x_1}(x_{k+1}) & X = (k+1, x_1) \quad (30b) \\ 0 & \text{otherwise.} \quad (30c) \end{cases}$$

where x_{k+1} is a target state. That is, this single-target transition density simply keeps the target state at time step $k+1$ of the trajectory, which corresponds to x_2 if $X = (k, x_{1:2})$ and to x_1 if $X = (k+1, x_1)$. When we apply a prediction step using this transition model to the updated PMBM on the set of trajectories, the result is a PMBM on the set of targets at time step $k+1$ that discards trajectory information at time step k.

Lemma 3 (TM-PMBM marginalisation)**.** *Given the updated PMBM density on the set of two-step trajectories between time steps k and $k+1$ of the form (14), the PMBM density over the set of target states is of the form (10) [37], with PPP intensity*

$$\lambda_{k+1|k+1}^M(x_{k+1}) = \left\langle \lambda_{k+1|k+1}, g_{k+1}^M(x_{k+1}|\cdot) p_{k+1}^{S,M}(\cdot) \right\rangle, \quad (31)$$

and Bernoulli components $f_{k+1|k+1}^{i,a^i,M}(\cdot)$, $i \in \{1, \ldots, n_{k+1|k+1}\}$, $a^i \in \{1, \ldots, h_{k+1|k+1}^i\}$, with probability of existence

$$r_{k+1|k+1}^{i,a^i,M} = r_{k+1|k+1}^{i,a^i} \left\langle p_{k+1|k+1}^{i,a^i}, p_{k+1}^{S,M} \right\rangle \quad (32)$$

and single-target density

$$p_{k+1|k+1}^{i,a^i,M}(x_{k+1}) = \frac{\left\langle p_{k|k}^{i,a^i}, g_{k+1}^M(x_{k+1}|\cdot) p_{k+1}^{S,M}(\cdot) \right\rangle}{\left\langle p_{k|k}^{i,a^i}, p_{k+1}^{S,M} \right\rangle}. \quad (33)$$

IV. Gaussian TM-PMBM filter

In this section, we present the Gaussian implementation of the TM-PMBM filter. Section IV-A outlines the assumptions underlying the Gaussian implementation. Section IV-B details the prediction step for both the PPP and Bernoulli components. Finally, Section IV-C provides the equations for the update step, addressing detection, missed detection, and new-birth hypotheses. The pseudocode of the TM-PMBM filter is given in Algorithm 1.

A. Preliminaries

From [39], we use the notation

$$\mathcal{N}(t, x_{1:\nu}; k, \overline{x}, P) = \begin{cases} \mathcal{N}(x_{1:\nu}; \overline{x}, P) & t = k,\ \nu = \iota \quad (34a) \\ 0 & \text{otherwise} \quad (34b) \end{cases}$$

to represent a trajectory Gaussian density with start time k and number of states ι, where $\iota = \dim(\overline{x})/n_x$. The mean $\overline{x} \in \mathbb{R}^{n_x \iota}$ and covariance matrix $P \in \mathbb{R}^{n_x \iota \times n_x \iota}$ are defined according to the length of the trajectory. The notation (34) can also be applied to trajectory measurements defined in the space $M_{(k+1)}$.

For the Gaussian implementation we make the following assumptions:

- The probability of survival is constant $p^S(x) = p^S$.
- The probability of detection is constant $p^D(X_{k+1}) = p^D$.
- The transition density is Gaussian $g(\cdot|x) = \mathcal{N}(\cdot; Fx, Q)$, where $F, Q \in \mathbb{R}^{n_x \times n_x}$.
- H is an $n_z \times n_x$ matrix defining the measurement model for a single target state and point detection.
- R is an $n_x \times n_x$ covariance matrix of the measurement noise for a single target state and point detection.
- A two-step trajectory X generates a trajectory measurement Z according to (9), where

  $$h_{\mu,\tau}(z_{1:\iota}|x_{1:\nu}) = \mathcal{N}(z_{1:\iota}; H_{\mu,\tau} x_{1:\nu}, R_\iota),$$

  with $R_\iota = I_\iota \otimes R$, $\iota = 1$ for $\mu \in 1, 2$ and $\iota = 2$ for $\mu = 3$, and $H_{\mu,\tau}$ is

  $$H_{\mu,\tau} = \begin{cases} [1,0] \otimes H & \mu = 1, \tau = 3 \quad (35a) \\ [0,1] \otimes H & \mu = 2, \tau = 3 \quad (35b) \\ I_2 \otimes H & \mu = 3, \tau = 3 \quad (35c) \\ H & \mu = 1, \tau = 1 \quad (35d) \\ H & \mu = 2, \tau = 2 \quad (35e) \\ 0 & \text{otherwise.} \quad (35f) \end{cases}$$

- The intensity of new born trajectories is

  $$\lambda_{k+1}^B(X_{k+1}) = \sum_{q_b=1}^{n_{k+1}^b} w_{k+1}^{b,q_b} \mathcal{N}(X_{k+1}; k+1, \overline{x}_{k+1}^{b,q_b}, P_{k+1}^{b,q_b}), \quad (36)$$

where n_{k+1}^b is the number of components, w_{k+1}^{b,q_b} is the weight of the q_b-th component, $\overline{x}_{k+1}^{b,q_b} \in \mathbb{R}^{n_x}$ its mean and $P_{k+1}^{b,q_b} \in \mathbb{R}^{n_x \times n_x}$ its covariance matrix. That is, new born trajectories have length 1 with probability one.

Given these assumptions, the PPP intensity on a target state x is a Gaussian mixture

$$\lambda_{k|k}^M(x) = \sum_{q=1}^{n_{k+1|k'}^p} w_{k|k}^{p,q} \mathcal{N}(x; \overline{x}_{k|k}^{p,q,M}, P_{k|k}^{p,q,M}), \tag{37}$$

where $w_{k|k}^{p,q} > 0$, $\overline{x}_{k|k}^{p,q,M} \in \mathbb{R}^{n_x}$ and $P_{k|k}^{p,q,M} \in \mathbb{R}^{n_x \times n_x}$. The PPP intensity on a two-step trajectory X at time step $k+1$, given the measurements up to $k' = k, k+1$, is a Gaussian mixture

$$\lambda_{k+1|k'}(X) = \sum_{q=1}^{n_{k+1|k'}^p} w_{k+1|k'}^{p,q} \mathcal{N}(X; t_{k+1|k'}^{p,q}, \overline{x}_{k+1|k'}^{p,q}, P_{k+1|k'}^{p,q}), \tag{38}$$

where $n_{k+1|k'}^p$ is the number of components, $t_{k+1|k'}^{p,q} \in \{k, k+1\}$, $w_{k+1|k'}^{p,q}$ is the weight of the q-th component, $\overline{x}_{k+1|k'}^{p,q} \in \mathbb{R}^{2n_x}$ and $P_{k+1|k'}^{p,q} \in \mathbb{R}^{2n_x \times 2n_x}$.

Furthermore, the Bernoulli component $f_{k+1|k'}^{i,a^i}(\cdot)$, $i \in \{1, \ldots, n_{k+1|k'}\}$, $a^i \in \{1, \ldots, h_{k+1|k'}^i\}$, on a target state x has a single-target density

$$p_{k|k}^{i,a^i,M}(x) = \mathcal{N}(x; \overline{x}_{k|k}^{i,a^i,M}, P_{k|k}^{i,a^i,M}). \tag{39}$$

The correspondent Bernoulli component on a two-step trajectory X has a single-trajectory density

$$p_{k+1|k'}^{i,a^i}(X) = \sum_{l=1}^{2} \beta_{k+1|k'}^{i,a^i}(l) \mathcal{N}(X; k, \overline{x}_{k+1|k'}^{i,a^i}(l), P_{k+1|k'}^{i,a^i}(l)), \tag{40}$$

where $\beta_{k+1|k'}^{i,a^i}(l)$ represents the probability that the corresponding trajectory terminates at time step k when $l = 1$, or survives until time step $k+1$ when $l = 2$, and $\overline{x}_{k+1|k+1}^{i,a^i}(l) \in \mathbb{R}^{ln_x}$ and $P_{k+1|k+1}^{i,a^i}(l) \in \mathbb{R}^{ln_x \times ln_x}$. We denote the components of the mean vector and covariance matrix as

$$\overline{x}_{k+1|k'}^{i,a^i}(2) = \begin{bmatrix} \overline{x}_{k+1|k'}^{i,a^i,1}(2) \\ \overline{x}_{k+1|k'}^{i,a^i,2}(2) \end{bmatrix} \tag{41}$$

$$P_{k+1|k'}^{i,a^i}(2) = \begin{bmatrix} P_{k+1|k'}^{i,a^i,1,1}(2) & P_{k+1|k'}^{i,a^i,1,2}(2) \\ P_{k+1|k'}^{i,a^i,2,1}(2) & P_{k+1|k'}^{i,a^i,2,2}(2) \end{bmatrix} \tag{42}$$

for cases with $l = 2$ in (40).

B. Prediction

Based on Lemma 1, we compute the prediction step in the Gaussian implementation. As in the standard TPMBM/TPMB filter implementations, in the PPP, we only consider alive trajectories [39].

Lemma 4 (Gaussian TM-PMBM prediction)**.** *Assume the filtering density at time step k is a PMBM on the set of target states of the form (10), with PPP intensity of the form (37). According to the transition density (7), the predicted intensity (16) is a Gaussian mixture intensity*

$$\lambda_{k+1|k}(X_{k+1}) = \underbrace{\sum_{q_b=1}^{n_{k+1}^b} w_{k+1}^{b,q_b} \mathcal{N}(X_{k+1}; k+1, \overline{x}_{k+1}^{b,q_b}, P_{k+1}^{b,q_b})}_{\lambda_{k+1}^B(X_{k+1})} + \sum_{q_p=1}^{n_{k+1|k}^p} w_{k+1|k}^{p,q_p} \mathcal{N}(X_{k+1}; k, \overline{x}_{k+1|k}^{p,q_p}, P_{k+1|k}^{p,q_p}), \tag{43}$$

where $n_{k+1|k}^p = n_k^b + n_{k|k}^p$, w_{k+1}^{b,q_b} and $w_{k+1|k}^{p,q_p}$ are the weights of the q_b-th and q_p-th components, with

$$w_{k+1|k}^{p,q_p} = w_{k|k}^{p,q_p} p^S, \tag{44}$$

and $\overline{x}_{k+1|k}^{p,q_p}$ and $P_{k+1|k}^{p,q_p}$ are the mean and covariance for surviving trajectories

$$\overline{x}_{k+1|k}^{p,q_p} = \begin{bmatrix} \overline{x}_{k|k}^{p,q_p,M} \\ F\overline{x}_{k|k}^{p,q_p,M} \end{bmatrix} \tag{45}$$

$$P_{k+1|k}^{p,q_p} = \begin{bmatrix} P_{k|k}^{p,q_p,M} & P_{k|k}^{p,q_p,M} F^T \\ F P_{k|k}^{p,q_p,M} & F P_{k|k}^{p,q_p,M} F^T + Q \end{bmatrix}, \tag{46}$$

while the mean $\overline{x}_{k+1}^{b,q_b}$ and covariance P_{k+1}^{b,q_b} for new born trajectories are defined in (36).

Assume the Bernoulli component $f_{k|k}^{i,a^i}(\cdot)$, $i \in \{1, \ldots, n_{k|k}\}$, $a^i \in \{1, \ldots, h_{k|k}^i\}$ is defined by $r_{k|k}^{i,a^i,M}$ and single-target density in the form of (39). According to (17) and (18), the predicted Bernoulli component $f_{k+1|k}^{i,a^i}(\cdot)$ has single-target density of the form (40) with

$$r_{k+1|k}^{i,a^i} = r_{k|k}^{i,a^i,M} \tag{47}$$

$$\beta_{k+1|k}^{i,a^i}(l) = \begin{cases} 1 - p^S & l = 1 \\ p^S & l = 2 \end{cases} \tag{48}$$

$$\overline{x}_{k+1|k}^{i,a^i}(1) = \overline{x}_{k|k}^{i,a^i,M} \tag{49}$$

$$P_{k+1|k}^{i,a^i}(1) = P_{k|k}^{i,a^i,M} \tag{50}$$

$$\overline{x}_{k+1|k}^{i,a^i}(2) = \begin{bmatrix} \overline{x}_{k|k}^{i,a^i,M} \\ F\overline{x}_{k|k}^{i,a^i,M} \end{bmatrix} \tag{51}$$

$$P_{k+1|k}^{i,a^i}(2) = \begin{bmatrix} P_{k|k}^{i,a^i,M} & P_{k|k}^{i,a^i,M} F^T \\ F P_{k|k}^{i,a^i,M} & F P_{k|k}^{i,a^i,M} F^T + Q \end{bmatrix}. \tag{52}$$

C. Update

Building on Lemma 2, we compute the update step in the Gaussian implementation.

Lemma 5 (Gaussian TM-PMBM update)**.** *Assume the PMBM density (14) on the set of two-step trajectories $\mathbf{X}_{k+1}$ with $\lambda_{k+1|k}(\cdot)$ of the form (43), and Bernoulli components $f_{k+1|k}^{i,a^i}(\cdot)$, $i \in \{1, \ldots, n_{k+1|k}\}$, $a^i \in \{1, \ldots, h_{k+1|k}^i\}$, with single trajectory density $p_{k+1|k}^{i,a^i}(\cdot)$ of the form (40). Then,*

the updated density with the set of trajectory measurements $\mathbf{Z}_{k+1} = \{Z_{k+1}^1, \ldots, Z_{k+1}^{m_{k+1}}\}$ *is a PMBM with PPP intensity*

$$\begin{aligned}\lambda_{k+1|k+1}(X_{k+1}) &= (1-p^D)\lambda_{k+1|k}(X_{k+1}) \\ &= \underbrace{(1-p^D)\sum_{q_b=1}^{n_{k+1}^b} w_{k+1}^{b,q_b}\mathcal{N}(X_{k+1}; k+1, \overline{x}_{k+1}^{b,q_b}, P_{k+1}^{b,q_b})}_{\textit{non-detected new-born trajectories}} \\ &\quad + \underbrace{\sum_{q_p=1}^{n_{k+1|k}^p} w_{k+1|k+1}^{p,q_p}\mathcal{N}(X_{k+1}; k, \overline{x}_{k+1|k}^{p,q_p}, P_{k+1|k}^{p,q_p})}_{\textit{non-detected surviving trajectories}}, \end{aligned} \tag{53}$$

where

$$w_{k+1|k+1}^{p,q_p} = (1-p^D)w_{k+1|k}^{p,q_p}. \tag{54}$$

The updated single-trajectory densities of the Bernoulli components $p_{k+1|k+1}^{i,a^i}(\cdot)$ *have the form (40). The missed detection hypothesis for the Bernoulli component* $f_{k+1|k}^{i,a^i}(\cdot)$ *has*

$$w_{k+1|k+1}^{i,a^i} = 1 - r_{k+1|k}^{i,a^i}p^D \tag{55}$$

$$r_{k+1|k+1}^{i,a^i} = \frac{r_{k+1|k}^{i,a^i}(1-p^D)}{1 - r_{k+1|k}^{i,a^i}p^D}, \tag{56}$$

and the two components in the mixture (40), corresponding to $l = \{1, 2\}$*, have the following parameters*

$$\beta_{k+1|k+1}^{i,a^i}(l) = \beta_{k+1|k}^{i,a^i}(l) \tag{57}$$

$$\overline{x}_{k+1|k+1}^{i,a^i}(l) = \overline{x}_{k+1|k}^{i,a^i}(l) \tag{58}$$

$$P_{k+1|k+1}^{i,a^i}(l) = P_{k+1|k}^{i,a^i}(l). \tag{59}$$

The detection hypothesis for the existing Bernoulli component $f_{k+1|k}^{i,\widetilde{a}^i}(\cdot)$ *and trajectory measurement* $Z^j = (t, z_{1:\iota})$ *is denoted with index* $a^i = \widetilde{a}^i + h_{k+1|k}^i j$*, where* $i \in \{1, \ldots, n_{k+1|k}\}$*,* $\widetilde{a}^i \in \{1, \ldots, h_{k+1|k}^i\}$ *and* $j \in \{1, \ldots, m_k\}$*. We proceed to explain the update for the different types of measurements.*

If $Z^j = (k, z_1) \in M_{(k+1)}^1$*, then based on (9a) and (9d), both the components* $l \in \{1, 2\}$ *in the mixture (40) are non-zero with parameters*

$$\begin{aligned} w_{k+1|k+1}^{i,a^i} &= r_{k+1|k}^{i,\widetilde{a}^i}p^D\left(\beta_{k+1|k}^{i,\widetilde{a}^i}(1) + \beta_{k+1|k}^{i,\widetilde{a}^i}(2)\,\gamma\right) \\ &\quad \times \mathcal{N}(Z; k, \overline{z}^{i,a^i}(1), S_{i,a^i}(1)) \end{aligned} \tag{60}$$

$$\beta_{k+1|k+1}^{i,a^i}(l) \propto \begin{cases} \beta_{k+1|k}^{i,\widetilde{a}^i}(1) & l = 1 \\ \beta_{k+1|k}^{i,\widetilde{a}^i}(2)\,\gamma & l = 2 \end{cases} \tag{61}$$

$$\overline{z}^{i,a^i}(l) = H_{1,\tau}\overline{x}_{k+1|k}^{i,\widetilde{a}^i}(l) \tag{62}$$

$$S_{i,a^i}(l) = H_{1,\tau}P_{k+1|k}^{i,\widetilde{a}^i}(l)H_{1,\tau}^T + R_1 \tag{63}$$

$$\begin{aligned} \overline{x}_{k+1|k+1}^{i,a^i}(l) &= \overline{x}_{k+1|k}^{i,\widetilde{a}^i}(l) \\ &\quad + P_{k+1|k}^{i,\widetilde{a}^i}(l)H_{1,\tau}^T S_{i,a^i}^{-1}(l)\left(z_1 - \overline{z}^{i,a^i}(l)\right) \end{aligned} \tag{64}$$

$$\begin{aligned} P_{k+1|k+1}^{i,a^i}(l) &= P_{k+1|k}^{i,\widetilde{a}^i}(l) \\ &\quad - P_{k+1|k}^{i,\widetilde{a}^i}(l)H_{1,\tau}^T S_{i,a^i}^{-1}(l)H_{1,\tau}P_{k+1|k}^{i,\widetilde{a}^i}(l), \end{aligned} \tag{65}$$

where $\tau = 1$ *for* $l = 1$ *and* $\tau = 3$ *for* $l = 2$*.*

If $Z^j = (k, z_{1:2}) \in M_{(k+1)}^3$*, then based on (9c), it follows that* $\beta_{k+1|k+1}^{i,a^i}(1) = 0$ *in (40), and the only non-zero component in the mixture (40) corresponds to* $l = 2$ *with parameters*

$$w_{k+1|k+1}^{i,a^i} = r_{k+1|k}^{i,\widetilde{a}^i}p_D\beta_{k+1|k}^{i,\widetilde{a}^i}(2)\widetilde{p}^D\mathcal{N}(Z; k, \overline{z}^{i,a^i}, S_{i,a^i}) \tag{66}$$

$$\beta_{k+1|k+1}^{i,a^i}(2) = 1 \tag{67}$$

$$\overline{z}^{i,a^i} = H_{3,3}\overline{x}_{k+1|k}^{i,\widetilde{a}^i}(2) \tag{68}$$

$$S_{i,a^i} = H_{3,3}P_{2,k+1|k}^{i,\widetilde{a}^i}H_{3,3}^T + R_2 \tag{69}$$

$$\begin{aligned} \overline{x}_{k+1|k+1}^{i,a^i}(2) &= \overline{x}_{k+1|k}^{i,\widetilde{a}^i}(2) \\ &\quad + P_{k+1|k}^{i,\widetilde{a}^i}(2)H_{3,3}^T S_{i,a^i}^{-1}\left(z_{1:2} - \overline{z}^{i,a^i}\right) \end{aligned} \tag{70}$$

$$\begin{aligned} P_{k+1|k+1}^{i,a^i}(2) &= P_{k+1|k}^{i,\widetilde{a}^i}(2) \\ &\quad - P_{k+1|k}^{i,\widetilde{a}^i}(2)H_{3,3}^T S_{i,a^i}^{-1}H_{3,3}P_{k+1|k}^{i,\widetilde{a}^i}(2). \end{aligned} \tag{71}$$

If $Z^j = (k+1, z_1) \in M_{(k+1)}^2$*, then based on (9b), it follows that* $\beta_{k+1|k+1}^{i,a^i}(1) = 0$ *in (40), and the only non-zero component in the mixture (40) corresponds to* $l = 2$ *with parameters*

$$w_{k+1|k+1}^{i,a^i} = r_{k+1|k}^{i,\widetilde{a}^i}p^D\beta_{k+1|k}^{i,\widetilde{a}^i}(2)\gamma\mathcal{N}(Z; k+1, \overline{z}^{i,a^i}, S_{i,a^i}) \tag{72}$$

$$\beta_{k+1|k+1}^{i,a^i}(2) = 1 \tag{73}$$

$$\overline{z}^{i,a^i} = H_{2,3}\overline{x}_{k+1|k}^{i,\widetilde{a}^i}(2) \tag{74}$$

$$S_{i,a^i} = H_{2,3}P_{k+1|k}^{i,\widetilde{a}^i}(2)H_{2,3}^T + R_1 \tag{75}$$

$$\begin{aligned} \overline{x}_{k+1|k+1}^{i,a^i}(2) &= \overline{x}_{k+1|k}^{i,\widetilde{a}^i}(2) \\ &\quad + P_{k+1|k}^{i,\widetilde{a}^i}(2)H_{2,3}^T S_{i,a^i}^{-1}\left(z_1 - \overline{z}^{i,a^i}\right) \end{aligned} \tag{76}$$

$$\begin{aligned} P_{k+1|k+1}^{i,a^i}(2) &= P_{k+1|k}^{i,\widetilde{a}^i}(2) \\ &\quad - P_{k+1|k}^{i,\widetilde{a}^i}(2)H_{2,3}^T S_{i,a^i}^{-1}H_{2,3}P_{k+1|k}^{i,\widetilde{a}^i}(2). \end{aligned} \tag{77}$$

For a new Bernoulli component $f_{k+1|k+1}^{i,a^i}(\cdot)$*,* $i \in \{n_{k+1|k}+j\}$*,* $j \in \{1, \ldots, m_{k+1}\}$*, initiated by the trajectory measurement* $Z^j = (t, z_{1:\nu}) \in M_{(k+1)}^\mu$*,* $\mu \in \{1, 2, 3\}$*, the first hypothesis expresses a missed detection and has parameters* $w_{k+1|k+1}^{i,1} = 1$*,* $r_{k+1|k+1} = 0$*. For the second hypothesis, we first calculate* $\left\langle \lambda_{k+1|k}, l\left(Z^j|\cdot\right)p^D\right\rangle$ *in (26) for each intensity component in the two mixtures (53). The result of the inner product* $\left\langle \lambda_{k+1|k}^B, l\left(Z^j|\cdot\right)p^D\right\rangle$ *involving the* q_b*-th component of the first mixture in (53) is denoted as* v^{b,q_b}*, and the result of the* q_p*-th component from the second mixture in (53) is denoted as* v^{p,q_p}*. For a component of the first mixture, we have*[1]

$$v^{b,q_b} = w_{k+1|k}^{b,q_b}p^D\mathcal{N}(z_1; H_{2,2}\overline{x}_{k+1|k}^{b,q_b}, S_{b,q_b}) \tag{78}$$

$$S_{b,q_b} = H_{2,2}P_{k+1|k}^{b,q_b}H_{2,2}^T + R_1, \tag{79}$$

[1]Note that the weight of the Poisson components is not included in (58) in [39] due to a typographical error. It is correctly included in (78) and (80).

and, for a component of the second mixture, the inner product is

$$v^{p,q_p} = \begin{cases} w_{k+1|k}^{p,q_p} p^D \gamma \mathcal{N}(z_1; H_{\widetilde{\mu},3}\overline{x}_{k+1|k}^{p,q_p}, S_{p,q_p,\widetilde{\mu}}) & Z^j \in M_{(k+1)}^{\widetilde{\mu}} \\ w_{k+1|k}^{p,q_p} p^D \widetilde{p}^D \mathcal{N}(z_2; H_{3,3}\overline{x}_{k+1|k}^{p,q_p}, S_{p,q_p,3}), & Z^j \in M_{(k+1)}^{3}, \end{cases} \tag{80}$$

where $\widetilde{\mu} \in \{1,2\}$ *and*

$$S_{p,q_p,\mu} = \begin{cases} H_{\mu,3} P_{k+1|k}^{b,q_b} H_{\mu,3}^T + R_1 & \mu = \widetilde{\mu} \in \{1,2\} \\ H_{3,3} P_{k+1|k}^{b,q_b} H_{3,3}^T + R_2 & \mu = 3. \end{cases} \tag{81}$$

Then, we compute $q_b^* = \max_{q_b} \left(v^{b,q_b}\right)$, $q_p^* = \max_{q_p} \left(v^{p,q_p}\right)$ *and set*

$$w_{k+1|k+1}^{i,2} = \lambda^C \left(Z^j\right) + \sum_{q_b=1}^{n_{k+1|k}^b} v^{b,q_b} + \sum_{q_p=1}^{n_{k+1}^p} v^{p,q_p} \tag{82}$$

$$r_{k+1|k+1}^{i,2} = \frac{\sum_{q_b=1}^{n_{k+1|k}^b} v^{b,q_b} + \sum_{q_p=1}^{n_{k+1}^p} v^{p,q_p}}{w_{k+1|k+1}^{i,2}} \tag{83}$$

$$p_{k+1|k+1}^{i,2}(X_{k+1}) = \mathcal{N}\left(X_{k+1}; t^{i,2}, \overline{x}_{k+1|k+1}^{i,2}, P_{k+1|k+1}^{i,2}\right). \tag{84}$$

If $v^{b,q_b^*} > v^{p,q_p^*}$, $t^{i,2} = k+1$ *and we set*

$$\overline{x}_{k+1|k+1}^{i,2} = \overline{x}_{k+1|k}^{b,q_b^*} + P_{k+1|k}^{b,q_b^*} H_{2,2} S_{b,q_b^*}^{-1} (z_1 - H_{2,2}\overline{x}_{k+1|k}^{b,q_b^*}) \tag{85}$$

$$P_{k+1|k+1}^{i,2} = P_{k+1|k}^{b,q_b^*} - P_{k+1|k}^{b,q_b^*} H_{2,2}^T S_{b,q_b^*}^{-1} H_{2,2} P_{k+1|k}^{b,q_b^*}, \tag{86}$$

based on (9e). If $v^{b,q_b^*} < v^{p,q_p^*}$, *the measurement model takes the form of (9c)-(9b),* $t^{i,2} = k$ *and* $\overline{x}_{k+1|k+1}^{i,2}$, $P_{k+1|k+1}^{i,2}$ *are given by substituting* $\overline{x}_{k+1}^{p,q_p^*}$ *and* P_{k+1}^{p,q_p^*} *into (64)-(65), (70)-(71) and (76)-(77) for* $Z^j \in M_{(k+1)}^1$, $Z^j \in M_{(k+1)}^3$ *and* $Z^j \in M_{(k+1)}^2$, *respectively.*

The proof of Lemma 5 is given in Appendix A. Note that if the measurement is detected only at time step k, the component correspondent to $l = 1$ in (40), defined by (61)-(65), will be discarded after the marginalisation step, and that $\beta_{k+1|k}^{i,\widetilde{a}^i}(1) + \beta_{k+1|k}^{i,\widetilde{a}^i}(2) = 1$. Furthermore, from (28), the single trajectory density of the new Bernoulli components is a Gaussian mixture of two-step trajectories with start times $t^{i,2} \in \{k, k+1\}$. To improve the filter's computational efficiency, we use a Gaussian approximation by defining (84) based on the Gaussian component with the highest weight in the mixture.

D. Marginalisation

Following Lemma 3, we compute the marginalisation step in the Gaussian implementation.

Lemma 6 (Gaussian TM-PMBM marginalisation)**.** *Assume the updated density at time step* k *and* $k+1$ *is a PMBM on the set of two-step trajectories of the form (14), with* $\lambda_{k+1|k+1}(\cdot)$ *of the form (43) and Bernoulli components* $f_{k+1|k+1}^{i,a^i}(\cdot)$, $i \in \{1, \ldots, n_{k+1|k+1}\}$, $a^i \in \{1, \ldots, h_{k+1|k+1}^i\}$, *with single trajectory density* $p_{k+1|k+1}^{i,a^i}(\cdot)$ *of the form (40). The updated density over the set of target states is a PMBM of the form (10), with PPP intensity*

$$\lambda_{k+1|k+1}^M(x_{k+1}) = (1-p^D) \sum_{q_b=1}^{n_{k+1}^b} w_{k+1}^{b,q_b} \mathcal{N}(x_{k+1}; \overline{x}_{k+1}^{b,q_b}, P_{k+1}^{b,q_b}) + \sum_{q_p=1}^{n_{k+1|k}^p} w_{k+1|k+1}^{p,q_p} \mathcal{N}(x_{k+1}; \overline{x}_{k+1|k}^{p,q_p,M}, P_{k+1|k}^{p,q_p,M}), \tag{87}$$

where $\overline{x}_{k+1|k}^{p,q_p,M} = \overline{x}_{k+1|k}^{p,q_p,2} \in \mathbb{R}^{n_x}$ *and* $P_{k+1|k}^{p,q_p,M} = P_{k+1|k}^{p,q_p,2,2} \in \mathbb{R}^{n_x \times n_x}$ *are the mean vector and covariance matrix at time step* $k+1$, *see (41) and (42). Based on Lemma 3, the Bernoulli components of the posterior density after the marginalisation* $f_{k+1|k+1}^{i,a^i,M}(\cdot)$, $i \in \{1, \ldots, n_{k+1|k+1}\}$, $a^i \in \{1, \ldots, h_{k+1|k+1}^i\}$ *have probability of existence*

$$r_{k+1|k+1}^{i,a^i,M} = r_{k+1|k+1}^{i,a^i} \beta_{k+1|k+1}^{i,a^i}(2), \tag{88}$$

and single-target density

$$p_{k+1|k+1}^{i,a^i,M}(x_{k+1}) = \mathcal{N}(x_{k+1}; \overline{x}_{k+1|k+1}^{i,a^i,M}, P_{k+1|k+1}^{i,a^i,M}), \tag{89}$$

Algorithm 1 Pseudocode of the TM-PMBM filter.

Input: Parameters of the TM-PMBM posterior at the previous time step, see Sec. IV-B, and set of trajectory measurements $\mathbf{Z}_{k+1}$ at current time window.
Output: Parameters of the TM-PMBM posterior at the current time window.

- Perform prediction, see Lemma 4.
- Update the PPP intensity (misdetection) (53)-(54).
for $Z \in \mathbf{Z}_{k+1}$ **do** ▷ Targets detected for the first time
  - Perform gating of Z w.r.t. Gaussian components of Poisson prior (43).
  if Z within the gate of at least one PPP component **then**
    - Create a new Bernoulli component (82)-(86) computing v^{b,q_b^*} and v^{p,q_p^*}.
  end if
end for
for $i = 1$ to $n_{k+1|k}$ **do** ▷ Go through all possible targets
  for $j_i = 1$ to h^i **do**
▷ h^i is the number of single-target hypotheses for target i
    - Create new misdetection hypothesis (55)-(59).
    - Perform gating on Z and form detection hypotheses by trajectory type (60)-(77).
  end for
end for
- Form the updated global hypotheses, see [15, Sec. V-C3].
- Marginalise PPP intensity (87) and Bernoulli components (88)-(90).
- Estimate target states by selecting the global hypothesis with the highest weight, see [15, Sec. VI-A].
- Prune low-weigth Poisson components, low-weight global hypotheses and Bernulli components with low probability of existence.

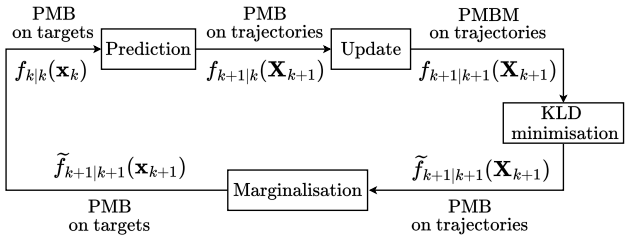

Figure 3: Diagram of the PMB filter based on trajectory measurements, the TM-PMB filter. The PMB density on the two-step trajectories is computed via KLD minimisation (with auxiliary variables [39]) of the PMBM posterior obtained from the update step performed with trajectory measurements. The order of the KLD minimisation and the marginalisation step can be swapped without affecting the result.

where

$$\overline{x}^{i,a^i,M}_{k+1|k+1} = \overline{x}^{i,a^i,2}_{k+1|k+1}(2), \qquad P^{i,a^i,M}_{k+1|k+1} = P^{i,a^i,2,2}_{k+1|k+1}(2). \tag{90}$$

E. TM-PMB filter

In this section, we discuss the (track-oriented) TM-PMB filter, which operates similarly to the PMB filter [38]. It can be derived through KLD minimisation by introducing auxiliary variables in the update step, as in the derivation of the trajectory PMB filter [39]. Fig. 3 provides a diagram illustrating the operation of the TM-PMB filter.

The resulting equations for the KLD minimisation step are

$$\widetilde{\lambda}_{k|k}(X) = \lambda_{k|k}(X) \tag{91}$$

$$r^i_{k|k} = \sum_{a^i=1}^{h^i_{k|k}} \overline{w}^{i,a^i}_{k|k} r^{i,a^i}_{k|k} \tag{92}$$

$$p^i_{k|k}(X) = \frac{\sum_{a^i=1}^{h^i_{k|k}} \overline{w}^{i,a^i}_{k|k} r^{i,a^i}_{k|k} p^{i,a^i}_{k|k}(X)}{\sum_{a^i=1}^{h^i_{k|k}} \overline{w}^{i,a^i}_{k|k} r^{i,a^i}_{k|k}}, \tag{93}$$

where

$$\overline{w}^{i,a^i}_{k|k} = \sum_{b\in\mathcal{A}_{k|k}:b^i=a^i} w^b_{k|k}. \tag{94}$$

After completing the minimisation step, the marginalisation step described in Section III-C is performed to obtain the PMB posterior density on the set of target states.

V. Simulations

In this section, we assess the performance of the TM-PMBM filter[2] and compare it with the standard PMBM filter based on sets of targets [15], as well as the corresponding PMB approximations [38]. The PMBM and PMB filters on sets of targets (which we simply refer to as PMBM and PMB filters) process only a set of (standard) measurements at each time step. For that reason, they discard the part of the trajectory measurements that corresponds to the time step at the beginning of the time window and proceed with an adjusted probability of detection, $\overline{p}^D$ and clutter intensity $\lambda^C_2(\cdot)$. All units in this section are presented in the International System of Units (SI) for clarity in notation and they are omitted for brevity.

We have also tested PMBM/PMB filters that process point measurements obtained from decomposing the trajectory measurements (without removing any states). Nevertheless, this option implies that a target may generate at most two point detections at each time step and standard point-target PMBM/PMB filters do not work well in this setting (mainly due to an increase in false targets). Therefore, for clarity, the results from these PMBM/PMB filters are omitted.

The filter implementations use a threshold for pruning the Poisson components $\Gamma_p = 10^{-5}$, a threshold for pruning global hypotheses $\Gamma_{mbm} = 10^{-4}$, and a threshold for pruning Bernoulli components $\Gamma_b = 10^{-5}$. The maximum number of global hypotheses is set to $N_h = 200$, and ellipsoidal gating is applied independently to the both ends of the trajectory measurements with a threshold of $\Gamma_g = 9$. In the trajectory-based filters, a trajectory measurement is considered for the update if at least one of its locations falls within the respective gate. The estimation is carried out by selecting the global hypothesis with the highest weight and and reporting Bernoulli components that have an existence probability greater than 0.1 [15, Sec. VI.A]. These parameters have been empirically determined to achieve good performance, representing a reasonable trade-off between computational burden and accuracy. All filters were implemented using Murty's algorithm [43].

The evaluation is conducted in terms of root mean square (RMS) generalised optimal subpattern assignment metric (GOSPA) error ($\alpha = 2$, $c = 10$, $p = 2$) [44], which allows for the decomposition of the total error into localisation error, missed target error and false target error. We examine two scenarios characterised by different parameters and structures, depicted in Fig. 4a and 4b. For each scenario, we conduct multiple simulations with different probabilities $\widetilde{p}^D$ of receiving a full trajectory measurement given the detection of a full measurement, and varying values of mean number of clutter trajectory measurements per scan $\overline{\lambda}^C$. These simulations are evaluated across four different lengths of the time window N_w, specifically $N_w = \{2, 5, 7, 10\}$ time steps.

The simulations were conducted on a laptop featuring an Intel (R) Core(TM) i7-8850H clocked at 2.60 GHz and 16 GB RAM. The implementation utilised MATLAB for all components except Murty's algorithm, which was implemented in C++[3]. The reported results are averaged over 100 Monte Carlo (MC) runs.

A. Models

In the simulations, the motion of the targets follows a nearly constant velocity model [46], and the target states are sampled at a sampling interval of $T = 0.2$. The single target state is defined within a two-dimensional Cartesian coordinate system as $[p_{x,k}, v_{x,k}, p_{y,k}, v_{y,k}]^T$, where the first two components denote the position and velocity along the x-axis, and the last

[2]The MATLAB implementation will be made publicly available at https://github.com/mrcfon.

[3]We used the Murty's algorithm implementation in the tracker component library [45].

two denote those along the y-axis. In the filters, the parameters for the linear and Gaussian motion and measurement models are as follows:

$$F = I_2 \otimes \begin{pmatrix} 1 & \Delta \\ 0 & 1 \end{pmatrix} \quad Q = qI_2 \otimes \begin{pmatrix} \Delta^3/3 & \Delta^2/2 \\ \Delta^2/2 & \Delta \end{pmatrix} \tag{95}$$

$$H = I_2 \otimes \begin{pmatrix} 1 & 0 \end{pmatrix} \quad R = \sigma^2 I_2 \,, \tag{96}$$

where $\otimes$ is the Kronecker product, $q = 0.01$, $\sigma^2 = 0.1$, and Δ is the time interval, defined as a multiple of the sampling interval, i.e., $\Delta = TN_w$. In the following sections, we refer to the scaling factor N_w as the length of the time window to indicate the results obtained by running the filters with different time intervals Δ.

We set the probability of detection to $p^D = 0.9$ for the filters based on trajectory measurements in all the simulations. For the filters based on target states (PMBM/PMB), which only consider measurements at the end of the time window, the equivalent probability of detection is defined as $\overline{p}^D = p^D(1-\gamma)$. This represents the probability of detection multiplied by the probability of cases (9c) and (9b). Moreover, we set the probability of survival to the next time step to $p^{S,T} = 0.99$ and the probability of survival to the next time window is $p^S = \left(p_S^{S,T}\right)^{N_w}$.

1) Trajectory measurement clutter model: Clutter is a PPP on the trajectory measurement space $M_{(k+1)}$, with clutter intensity is

$$\lambda^C(Z_{k+1}) = \begin{cases} \overline{\lambda}_P^C f_C^{P,1}(Z_{k+1}) & Z_{k+1} \in M^1_{(k+1)} \quad (97a) \\ \overline{\lambda}_P^C f_C^{P,2}(Z_{k+1}) & Z_{k+1} \in M^2_{(k+1)} \quad (97b) \\ \overline{\lambda}_F^C f_C^{F}(Z_{k+1}) & Z_{k+1} \in M^3_{(k+1)}, \quad (97c) \end{cases}$$

where $\overline{\lambda}_F^C$ is the clutter rate for a trajectory measurement in $M^3_{(k+1)}$, and $\overline{\lambda}_P^C$ is the clutter rate for a trajectory measurement in $M^1_{(k+1)}$ or $M^2_{(k+1)}$. The spatial single measurement densities for full and partial trajectory measurements are

$$f_C^{P,1}(k, z_1) = f_C^{P,2}(k+1, z_1) = \begin{cases} \dfrac{1}{|V|} & z_1 \in V \quad (98a) \\ 0 & \text{otherwise}, \quad (98b) \end{cases}$$

$$f_C^{F}(t, z_{1:2}) = \begin{cases} 1/|V|^2 & z_{1:2} \in V \times V \quad (99a) \\ 0 & \text{otherwise}, \quad (99b) \end{cases}$$

where V is the area of the field of view of the sensor, and $|V|$ represents the volume/size of V. The spatial density (98) is uniform in V, and the spatial pdf (99) is uniform in $V \times V$.

The clutter rate is the integral on the single-trajectory measurement space [18]

$$\overline{\lambda}^C = \int \lambda^C(Z_{k+1})\, dZ_{k+1} \tag{100}$$

$$= \int \lambda^C(k, z_{1:2})\, dz_{1:2} + \int \lambda^C(k, z_1)\, dz_1 + \int \lambda^C(k+1, z_1)\, dz_1 \tag{101}$$

$$= \overline{\lambda}_F^C + 2\overline{\lambda}_P^C. \tag{102}$$

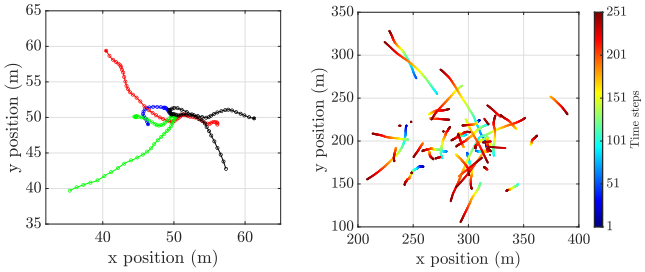

(a) Ground truth for Scenario 1, in which each target is represented by a distinct colour.

(b) Ground truth for Scenario 2, in which the colours represent the temporal evolution of the target positions.

Figure 4: Scenarios used to assess the performance of the TM-PMBM filter and to compare it with the standard PMBM filter. In Fig. 4a, target positions at $k = 1$ are marked with a cross, and subsequent positions are indicated every five time steps with circles.

In the simulations, the clutter rates of full and partial clutter trajectory measurements are equal, i.e, $\overline{\lambda}_F^C = \overline{\lambda}_P^C$.

The standard PMBM/PMB filters are defined on sets of targets. Therefore the clutter model proposed in (99-102) cannot be used with these filters. We define the clutter model for the PMBM/PMB filters by marginalising the PPP of the trajectory clutter model at time step k. This results in [37]

$$\lambda_2^C(z) = \left(\overline{\lambda}_F^C + \overline{\lambda}_P^C\right) f_C^{P,2}(k+1, z)\,. \tag{103}$$

B. Scenario 1

Scenario 1 extends the base scenario outlined in [15]. It involves four targets, all originating at time step $k = 1$ and remaining alive throughout a simulation of 250 time steps, except for one that dies at time step 125 (depicted in blue in Fig. 4a). This scenario is recognised as challenging due to the convergence of all targets around time step 125, when the blue one dies.

The targets are modelled as being born according to a PPP of intensity 3 at the first time step, and 0.005 at the next time steps. The intensity at each time step is Gaussian with mean $[50, 0, 50, 0]^T$, and covariance $\mathrm{diag}([50, 1, 50, 1]^2)$, which covers the considered area of $[0, 100] \times [0, 100]$. In each time window, we approximate the Gaussian mixture of new PPP components through Gaussian mixture reduction, resulting in a single component that represents all possible targets born within a time window.

We tested this scenario with two different probabilities of receiving a full trajectory measurement $\widetilde{p}^D$, specifically $\widetilde{p}^D \in \{0.7, 0.9\}$. The results are depicted, respectively, in Figs. 6 and 7. For each value of $\widetilde{p}^D$, we conducted three simulations with different clutter rates $\overline{\lambda}^C \in \{0.1, 1, 10\}$ for each of the following time window lengths: $N_w \in \{2, 5, 7, 10\}$.

Both the TM-PMBM and TM-PMB filters outperform the standard PMBM and PMB filters, respectively. Fig. 5 presents a comparison, based on a single MC run, of the tracking performance of TM-PMBM and standard PMBM filters. Figs. 6b and 7b demonstrate that the localisation errors tends to converge to a common value as the length of the time window

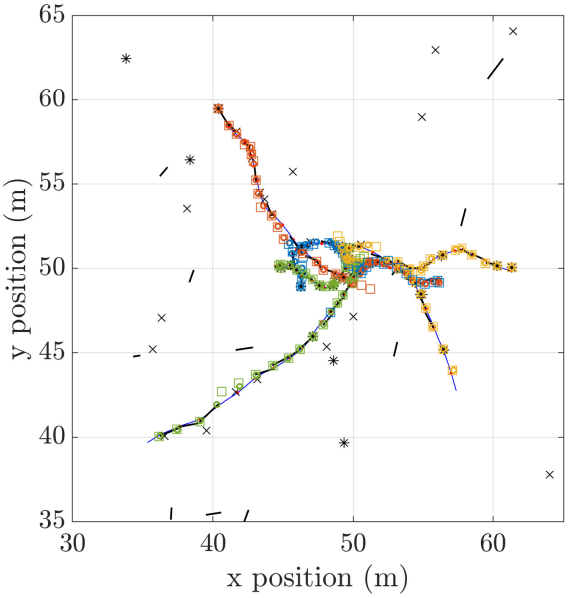

Figure 5: Comparison of the tracking performance of TM-PMBM (depicted with circle markers) and standard PMBM (depicted with square markers) filters based on Scenario 1, with $N_w = 7$, $\widetilde{p}^D = 0.7$ and $\overline{\lambda}^C = 10$. The ground-truth trajectories are shown in blue, while the red dots denote the ground-truth locations at the beginning and end of each time window. Measurements obtained across all time steps are shown in black: $Z \in M^1_{(k+1)}$ with crosses, $Z \in M^2_{(k+1)}$ with stars, and $Z = (k, z_{1:2}) \in M^3_{(k+1)}$ with bars connecting z_1 and z_2. At many time steps, the outputs of both filters are visually similar though at other time steps, the TM-PMBM clearly outperforms the standard PMBM.

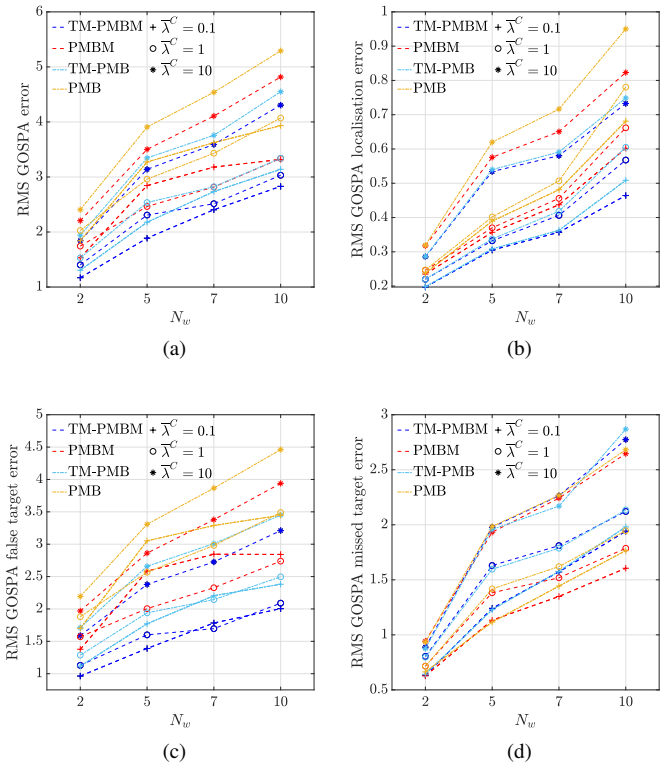

Figure 6: GOSPA metric results for Scenario 1 with $\widetilde{p}^D = 0.9$ and clutter rates $\overline{\lambda}^C = \{0.1, 1, 10\}$, averaged over 100 MC runs. Each filter is represented by a distinct colour, and simulations sharing the same clutter rate are identified using the same marker. Results for the TM-PMBM and PMBM filters are connected by dashed lines, while those for the TM-PMB and PMB filters are connected by dash-dotted lines.

decreases. Conversely, extending the duration of the time window results in higher localisation errors and a greater disparity in localisation accuracy between the TM-PMBM/TM-PMB filters and the standard ones.

The missed target error is quite similar between the TM-PMBM/TM-PMB filters and the conventional ones. However, the TM-PMBM/TM-PMB filters significantly outperform standard filters in the high clutter scenario, as shown in Fig. 6d for $\overline{\lambda}^C = 10$. Fig. 7d indicates that the difference in missed target error generally increases with a lower $\widetilde{p}^D$, especially for long time windows.

On the contrary, the TM-PMBM filter and the standard one have a similar false target error in the high clutter scenarios, as shown in Figs. 6c for $\overline{\lambda}^C = 10$. Note that for PMB filters, the difference remains significant and favours the TM-PMB filter. TM-PMBM and TM-PMB filters perform well even in a scenario with a lower $\widetilde{p}^D$, as shown in Fig. 7c. However, the best performance in the high clutter scenario is achieved by the standard PMBM.

Tab. I reports the computational times of the filters for each simulation, with the TM-PMBM/TM-PMB filters exhibiting lower computational times in scenarios with longer time windows. Although the standard PMBM/PMB filters typically operate with a larger number of single-target and global hypotheses, as showed in the hypothesis-count analysis presented in Appendix B, the TM-PMBM/TM-PMB filters do not always outperform the standard PMBM/PMB filters in terms of computational time, owing to the additional cost of marginalisation and the evaluation of Gaussian distributions in higher-dimensional spaces.

C. Scenario 2

Scenario 2 involves targets that appear and disappear at various time intervals within the area $A = [0, 600] \times [0, 400]$. The target state at the appearing time is Gaussian with mean $[300, 0, 200, 0]^T$ and covariance $\mathrm{diag}([30, 1, 30, 1]^2)$. The birth process follows a Poisson distribution with an average of 0.16 targets per time step, and the average lifespan of each target is 1000 seconds. The scenario has an average number of alive target at each time step $N_a = 20.32$, with a maximum of 45 targets present at the final time step. The PPP intensity at each is Gaussian with mean $[300, 0, 200, 0]^T$ and covariance $\mathrm{diag}([(300, 1, 200, 1]^2)$.

Fig. 8 presents the results in terms of RMS GOSPA error with $\widetilde{p}^D \in \{0.9, 0.7\}$ and clutter rates $\overline{\lambda}^C \in \{0.24, 2.4\}$. In both configurations, the performance of the TM-PMB filter is much more similar to that of the TM-PMBM one compared to the conventional filters. Overall, TM-PMBM and TM-PMB outperform their corresponding versions based on target states.

Table I: Computational times of the TM-PMBM/TM-PMB filters and the PMBM/PMB filters for simulations based on Scenario 1. For each scenario, the fastest filter between TM-PMBM/PMBM and TM-PMB/PMB is underlined.

		TM-PMBM with $N_w =$				PMBM with $N_w =$				TM-PMB with $N_w =$				PMB with $N_w =$			
$\widetilde{p}^D$	$\overline{\lambda}^C$	2	5	7	10	2	5	7	10	2	5	7	10	2	5	7	10
0.9	0.1	4.44	0.76	0.39	0.32	3.38	1.09	0.79	0.49	0.39	0.19	0.13	0.10	0.35	0.14	0.11	0.10
	1	6.15	1.16	0.60	0.57	4.48	1.79	1.18	0.66	0.45	0.25	0.17	0.13	0.51	0.17	0.16	0.12
	10	7.14	1.51	1.41	0.99	5.65	2.67	1.97	1.35	1.35	0.60	0.40	0.35	0.97	0.44	0.43	0.40
0.7	0.1	3.84	0.91	0.65	0.40	3.24	1.14	0.78	0.55	0.46	0.20	0.12	0.10	0.33	0.13	0.12	0.10
	1	6.10	1.27	1.01	0.65	4.54	2.08	1.27	0.73	0.54	0.26	0.16	0.14	0.42	0.18	0.26	0.14
	10	6.67	2.25	1.29	1.20	6.31	3.46	2.50	1.96	1.22	0.67	0.47	0.45	0.99	0.62	0.75	0.49

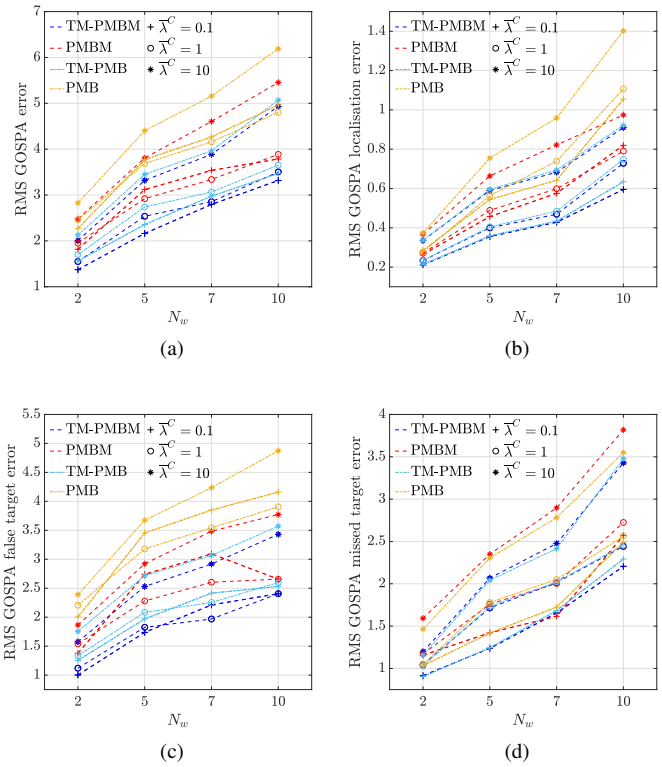

(a) (b) (c) (d)

Figure 7: GOSPA metric results for Scenario 1 with $\widetilde{p}^D = 0.7$ and clutter rates $\overline{\lambda}^C = \{0.1, 1, 10\}$, averaged over 100 MC runs. Each filter is represented by a distinct colour, and simulations sharing the same clutter rate are identified using the same marker. Results for the TM-PMBM and PMBM filters are connected by dashed lines, while those for the TM-PMB and PMB filters are connected by dash-dotted lines.

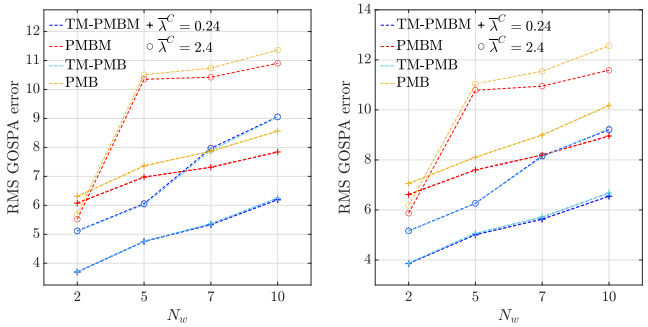

(a) $\widetilde{p}^D = 0.9$ (b) $\widetilde{p}^D = 0.7$

Figure 8: GOSPA metric results for Scenario 2 with $\widetilde{p}^D = \{0.9, 0.7\}$ and clutter rates $\overline{\lambda}^C = \{0.24, 2.4\}$, averaged over 100 Monte Carlo runs. Each filter is represented by a distinct colour, and simulations sharing the same clutter rate are identified using the same marker.

VI. Conclusions

In this paper, we have proposed a PMBM filter that processes sets of sensor measurements, in which each measurement represents a trajectory in a two-time step window. We have derived the filtering recursion by first performing the prediction step on the PMBM posterior density on the target states, followed by the update step with a set of trajectory measurements, which requires the use of the PMBM on the set of trajectories over the last two time steps. We have then marginalised the PMBM density to obtain a posterior on the target state estimation accuracy.

We have also introduced the TM-PMB approximation and a Gaussian implementation of the TM-PMBM filter suitable for linear/Gaussian measurement models. Finally, we compared the performance of the TM-PMBM and TM-PMB filters with their counterparts based on target states in two scenarios. The TM-PMBM and TM-PMB filters demonstrated superior performance in both scenarios.

Acknowledgements

The authors thank Sintela Ltd. and the EPSRC Centre for Doctoral Training in Distributed Algorithms for their support. Simon Maskell's work was supported by the Royal Academy of Engineering. The authors also thank Paul Horridge for his helpful discussions on a closely related issue.

References

[1] S. Blackman and R. Popoli, *Design and Analysis of Modern Tracking Systems*. Artech House, 1991.

[2] S. Maskell, "Statistical Methods for Target Tracking," in *Wiley Encyclopedia of Computer Science and Engineering*. John Wiley & Sons, Ltd, 2009, pp. 2820–2829.

[3] Y. Bar-Shalom, P. K. Willett, and X. Tian, *Tracking and Data Fusion: A Handbook of Algorithms*. YBS Publishing, 2011.

[4] M. I. Skolnik, *Introduction to Radar Systems*. McGraw-Hill, 1962.

[5] J. Choi, S. Ulbrich, B. Lichte, and M. Maurer, "Multi-Target Tracking using a 3D-Lidar sensor for autonomous vehicles," in *16th International IEEE Conference on Intelligent Transportation Systems (ITSC 2013)*, Oct. 2013, pp. 881–886, iSSN: 2153-0017.

[6] E. Maggio, M. Taj, and A. Cavallaro, "Efficient Multitarget Visual Tracking Using Random Finite Sets," *IEEE Transactions on Circuits and Systems for Video Technology*, vol. 18, no. 8, pp. 1016–1027, 2008.

[7] N. Chenouard, I. Bloch, and J. Olivo-Marin, "Multiple hypothesis tracking for cluttered biological image sequences," *IEEE Transactions on Pattern Analysis and Machine Intelligence*, vol. 35, no. 11, pp. 2736–3750, Nov. 2013.

[8] D. Reid, "An algorithm for tracking multiple targets," *IEEE Transactions on Automatic Control*, vol. 24, no. 6, pp. 843–854, Dec. 1979.

[9] T. Fortmann, Y. Bar-Shalom, and M. Scheffe, "Sonar tracking of multiple targets using joint probabilistic data association," *IEEE Journal of Oceanic Engineering*, vol. 8, no. 3, 1983.

[10] R. P. S. Mahler, *Advances in Statistical Multisource-Multitarget Information Fusion*. Artech House, 2014.

[11] J. Goutsias, R. P. S. Mahler, and H. T. Nguyen, *Random Sets: Theory and Applications*. Springer Science & Business Media, Dec. 2012.

[12] I. R. Goodman, R. P. Mahler, and H. T. Nguyen, *Mathematics of Data Fusion*. Springer Science & Business Media, Mar. 2013.

[13] I. Schlangen, E. D. Delande, J. Houssineau, and D. E. Clark, "A Second-Order PHD Filter With Mean and Variance in Target Number," *IEEE Transactions on Signal Processing*, vol. 66, no. 1, pp. 48–63, Jan. 2018.

[14] R. Mahler, "Multitarget Bayes filtering via first-order multitarget moments," *IEEE Transactions on Aerospace and Electronic Systems*, vol. 39, no. 4, pp. 1152–1178, Oct. 2003.

[15] Á. F. García-Fernández, J. L. Williams, K. Granström, and L. Svensson, "Poisson multi-Bernoulli mixture filter: direct derivation and implementation," *IEEE Transactions on Aerospace and Electronic Systems*, vol. 54, no. 4, pp. 1883–1901, 2018.

[16] Á. F. García-Fernández, Y. Xia, K. Granström, L. Svensson, and J. L. Williams, "Gaussian implementation of the multi-Bernoulli mixture filter," in *2019 22th International Conference on Information Fusion (FUSION)*, Jul. 2019, pp. 1–8.

[17] B. Vo and B. Vo, "Labeled Random Finite Sets and Multi-Object Conjugate Priors," *IEEE Transactions on Signal Processing*, vol. 61, no. 13, pp. 3460–3475, Jul. 2013.

[18] Á. F. García-Fernández and L. Svensson, "Trajectory PHD and CPHD Filters," *IEEE Transactions on Signal Processing*, vol. 67, no. 22, pp. 5702–5714, Nov. 2019.

[19] Á. F. García-Fernández, L. Svensson, and M. R. Morelande, "Multiple target tracking based on sets of trajectories," *IEEE Transactions on Aerospace and Electronic Systems*, vol. 56, no. 3, pp. 1685–1707, 2020.

[20] R. P. S. Mahler, *Statistical Multisource-Multitarget Information Fusion*. USA: Artech House, Inc., 2007.

[21] K. Granström, M. Baum, and S. Reuter, "Extended Object Tracking: Introduction, Overview, and Applications," *Journal of Advances in Information Fusion*, vol. 12, Dec. 2017.

[22] S. Davey, M. Rutten, and B. Cheung, "A comparison of detection performance for several Track-Before-Detect algorithms," in *2008 11th International Conference on Information Fusion*, Jun. 2008, pp. 1–8.

[23] M. Fontana, Á. F. García-Fernández, and S. Maskell, "Notch power detector for multiple vehicle trajectory estimation with distributed acoustic sensing," *Signal Processing*, vol. 232, p. 109905, Jul. 2025.

[24] L. R. Moyer, J. Spak, and P. Lamanna, "A Multi-Dimensional Hough Transform-Based Track-Before-Detect Technique for Detecting Weak Targets in Strong Clutter Backgrounds," *IEEE Transactions on Aerospace and Electronic Systems*, vol. 47, no. 4, pp. 3062–3068, 2011.

[25] S. Tonissen and Y. Bar-Shalom, "Maximum likelihood track-before-detect with fluctuating target amplitude," *IEEE Transactions on Aerospace and Electronic Systems*, vol. 34, no. 3, pp. 796–809, 1998.

[26] Y. Barniv and O. Kella, "Dynamic Programming Solution for Detecting Dim Moving Targets Part II: Analysis," *IEEE Transactions on Aerospace and Electronic Systems*, vol. AES-23, no. 6, pp. 776–788, Nov. 1987.

[27] B. Carlson, E. Evans, and S. Wilson, "Search radar detection and track with the Hough transform. I. system concept," *IEEE Transactions on Aerospace and Electronic Systems*, vol. 30, no. 1, pp. 102–108, 1994.

[28] P. V. C. Hough, *Method and means for recognizing complex patterns*, unknown, Ed. U.S. Patent 3,069,654, Dec 1962.

[29] R. O. Duda and P. E. Hart, "Use of the Hough transformation to detect lines and curves in pictures," *Communications of the ACM*, vol. 15, no. 1, pp. 11–15, Jan. 1972.

[30] M. A. Fischler and R. C. Bolles, "Random sample consensus: a paradigm for model fitting with applications to image analysis and automated cartography," *Communications of the ACM*, vol. 24, no. 6, pp. 381–395, Jun. 1981.

[31] A. P. Dempster, N. M. Laird, and D. B. Rubin, "Maximum Likelihood from Incomplete Data Via the EM Algorithm," *Journal of the Royal Statistical Society: Series B (Methodological)*, vol. 39, no. 1, pp. 1–22, 2018.

[32] J. Arnold, Y. Bar-Shalom, and R. Mucci, "Track Segment Association with a Distributed Field of Sensors," in *1984 American Control Conference*, Jun. 1984, pp. 605–612.

[33] M. Levesque and S. Buteau, "Image processing technique for automatic detection of satellite streaks," *Defense Research and Development Canada Valcartier (Quebec)*, 2007.

[34] A. Finelli, P. Willett, Y. Bar-Shalom, D. Melgaard, and R. Byrne, "Tracking of streaking targets in video frames," in *2017 IEEE Aerospace Conference*, Mar. 2017, pp. 1–10.

[35] S. Schoenecker, P. Willett, and Y. Bar-Shalom, "Maximum likelihood probabilistic multi-hypothesis tracker applied to multistatic sonar data sets," in *Signal Processing, Sensor Fusion, and Target Recognition XX*, I. Kadar, Ed., vol. 8050, International Society for Optics and Photonics. SPIE, 2011, p. 80500A.

[36] O. E. Drummond, "Hybrid sensor fusion algorithm architecture and tracklets," in *Signal and Data Processing of Small Targets 1997*, vol. 3163. SPIE, Oct. 1997, pp. 485–502.

[37] K. Granström, L. Svensson, Y. Xia, J. Williams, and Á. F. García-Fernández, "Poisson Multi-Bernoulli Mixtures for Sets of Trajectories," *IEEE Transactions on Aerospace and Electronic Systems*, vol. 61, no. 2, pp. 1–16, Apr. 2025.

[38] J. L. Williams, "Marginal multi-Bernoulli filters: RFS derivation of MHT, JIPDA, and association-based MeMBer," *IEEE Transactions on Aerospace and Electronic Systems*, vol. 51, no. 3, pp. 1664–1687, 2015.

[39] Á. F. García-Fernández, L. Svensson, J. L. Williams, Y. Xia, and K. Granström, "Trajectory Poisson multi-Bernoulli filters," *IEEE Transactions on Signal Processing*, vol. 68, pp. 4933–4945, 2020.

[40] Y. Xia, K. Granström, L. Svensson, Á. F. García-Fernández, and J. L. Williams, "Multi-Scan Implementation of the Trajectory Poisson Multi-Bernoulli Mixture Filter," *Journal of Advances in Information Fusion*, vol. 14, no. 2, pp. 213–235, Dec. 2019.

[41] K. Granström, L. Svensson, Y. Xia, J. Williams, and Á. F. García-Fernández, "Poisson Multi-Bernoulli Mixture Trackers: Continuity Through Random Finite Sets of Trajectories," in *2018 21st International Conference on Information Fusion (FUSION)*, Jul. 2018, pp. 1–5.

[42] Á. F. García-Fernández, J. L. Williams, L. Svensson, and Y. Xia, "A Poisson Multi-Bernoulli Mixture Filter for Coexisting Point and Extended Targets," *IEEE Transactions on Signal Processing*, vol. 69, pp. 2600–2610, 2021.

[43] K. G. Murty, "An Algorithm for Ranking all the Assignments in Order of Increasing Cost," *Operations Research*, vol. 16, no. 3, pp. 682–687, 1968.

[44] A. S. Rahmathullah, Á. F. García-Fernández, and L. Svensson, "Generalized optimal sub-pattern assignment metric," in *Proc. 20th Int. Conf. Information Fusion (Fusion)*, Jul. 2017, pp. 1–8.

[45] D. F. Crouse, "The tracker component library: free routines for rapid prototyping," *IEEE Aerospace and Electronic Systems Magazine*, vol. 32, no. 5, pp. 18–27, May 2017.

[46] Y. Bar-Shalom, X.-R. Li, and T. Kirubarajan, *Estimation with Applications to Tracking and Navigation*. John Wiley & Sons, Inc., 2001.

Supplementary material: Poisson multi-Bernoulli mixture filter for trajectory measurements

APPENDIX A

In this appendix, we prove the expression of the updated Bernoulli components in Lemma 5. For clarity, we simplify the notation in this section by omitting the dependence on $k+1$ of the single-trajectory measurements, single-trajectory state and related spaces.

A. Update of Bernoulli component

According to Lemma 4, the predicted Bernoulli component $f^{i,\widetilde{a}^i}_{k+1|k}(\cdot)$, $i \in \{1,\ldots,n_{k+1|k}\}$, $\widetilde{a}^i \in \{1,\ldots,h^i_{k+1|k}\}$ has single-target density of the form (40). Based on Lemma 2, the detection hypothesis for $f^{i,\widetilde{a}^i}_{k+1|k}(\cdot)$ and trajectory measurement $Z^j = (t, z_{1:\iota})$ is denoted as $f^{i,\widetilde{a}^i}_{k+1|k}(\cdot)$ with index $a^i = \widetilde{a}^i + h^i_{k+1|k} j$ and has parameters that depend on the inner product

$$\begin{aligned}
&\langle\, p^{i,\widetilde{a}^i}_{k+1|k}, l\left(Z^j_{k+1}|\cdot\right) p^D \rangle \\
&= p^D \int_{T^1 \uplus T^3} l\left(Z^j|X\right) p^{i,\widetilde{a}^i}_{k+1|k}(X)\, dX \qquad (104)\\
&= p^D \Big[\beta^{i,a^i}_{k+1|k}(1) \\
&\quad \times \int_{T^1} l\left(Z^j|X\right) \mathcal{N}(X; k, \overline{x}^{i,\widetilde{a}^i}_{k+1|k}(1), P^{i,\widetilde{a}^i}_{k+1|k}(1))dX \\
&\quad + \beta^{i,a^i}_{k+1|k}(2) \\
&\quad \times \int_{T^3} l\left(Z^j|X\right) \mathcal{N}(X; k, \overline{x}^{i,\widetilde{a}^i}_{k+1|k}(2), P^{i,\widetilde{a}^i}_{k+1|k}(2))dX\Big]. \qquad (105)
\end{aligned}$$

Note that the integral does not consider T^2 as these single-trajectory densities do not consider new born targets at time step $k+1$. We derive (105) for each possible trajectory measurement defined in (4).

1) Measurements detected only at time step k: If $Z^j = (k, z_1) \in M^1$, the measurement model takes the form of (9a) and (9d) for $X \in T^3$ and $X \in T^1$, respectively. Therefore, (105) yields two non-zero terms

$$\begin{aligned}
&\langle\, p^{i,\widetilde{a}^i}_{k+1|k}, l\left(Z^j_{k+1}|\cdot\right) p^D \rangle \\
&= p^D \Big[\beta^{i,a^i}_{k+1|k}(1) \\
&\quad \times \int_{\mathbb{R}^{n_x}} h_{1,1}(z_1|x_1)\mathcal{N}(x_1, \overline{x}^{i,\widetilde{a}^i}_{k+1|k}(1), P^{i,\widetilde{a}^i}_{k+1|k}(1))dx_1 \\
&\quad + \beta^{i,a^i}_{k+1|k}(2)\gamma \\
&\quad \times \int_{\mathbb{R}^{2n_x}} h_{1,3}(z_1|x_{1:2})\mathcal{N}(x_{1:2}, \overline{x}^{i,\widetilde{a}^i}_{k+1|k}(2), P^{i,\widetilde{a}^i}_{k+1|k}(2))dx_{1:2}\Big] \qquad (106)\\
&= p^D \Big[\beta^{i,a^i}_{k+1|k}(1) \\
&\quad \times \int_{\mathbb{R}^{n_x}} \mathcal{N}\left(z_1; H_{1,1}x_1, R_1\right)\mathcal{N}(x_1, \overline{x}^{i,\widetilde{a}^i}_{k+1|k}(1), P^{i,\widetilde{a}^i}_{k+1|k}(1))dx_1 \\
&\quad + \beta^{i,a^i}_{k+1|k}(2)\gamma \int_{\mathbb{R}^{2n_x}} \mathcal{N}\left(z_1; H_{1,3}x_{1:2}, R_1\right) \\
&\quad \times \mathcal{N}(x_{1:2}, \overline{x}^{i,\widetilde{a}^i}_{k+1|k}(2), P^{i,\widetilde{a}^i}_{k+1|k}(2))dx_1 dx_2\Big] \qquad (107)\\
&= p^D \Big[\beta^{i,a^i}_{k+1|k+1}(1)\mathcal{N}\left(z_1; \overline{z}^{i,a^i}(1), S_{i,a^i}(1)\right) \\
&\quad + \beta^{i,a^i}_{k+1|k+1}(2)\mathcal{N}\left(z_1; \overline{z}^{i,a^i}(2), S_{i,a^i}(2)\right)\Big] \qquad (108)
\end{aligned}$$

where

$$\overline{z}^{i,a^i}(l) = H(l)\overline{x}^{i,\widetilde{a}^i}_{k+1|k}(l) \qquad (109)$$

$$S_{i,a^i}(l) = H(l)P^{i,\widetilde{a}^i}_{k+1|k}(l)H^T(l) + R \qquad (110)$$

with $l \in \{1,2\}$, $H(1) = H_{1,1} = H$ and $H(2) = H_{1,3} = [1,0] \otimes H$. Therefore, $\overline{z}^{i,a^i}(1) = \overline{z}^{i,a^i}(2)$, $S_{i,a^i}(1) = S_{i,a^i}(2)$ and (108) yields (60). Based on (25), the Kalman update gives the parameters for the updated single-trajectory density of the form (40).

2) Measurement detected at both time steps k and $k+1$: If $Z^j = (k, z_{1:2}) \in M^3$, the measurement model takes the form of (9c) for $X \in T^3$, while it is zero for $X \in T^1$. Therefore, (105) yields a non-zero term corresponding to $l = 2$ in (40)

$$\begin{aligned}
&\langle\, p^{i,\widetilde{a}^i}_{k+1|k}, l\left(Z^j_{k+1}|\cdot\right) p^D \rangle \\
&= p^D \beta^{i,a^i}_{k+1|k}(2)\widetilde{p}^D \\
&\quad \times \int_{\mathbb{R}^{2n_x}} h_{3,3}(z_{1:2}|x_{1:2})\mathcal{N}(x_{1:2}, \overline{x}^{i,\widetilde{a}^i}_{k+1|k}(2), P^{i,\widetilde{a}^i}_{k+1|k}(2))dx_{1:2} \qquad (111)\\
&= p^D \beta^{i,a^i}_{k+1|k}(2)\widetilde{p}^D \int_{\mathbb{R}^{2n_x}} \mathcal{N}\left(z_{1:2}; H_{3,3}x_{1:2}, R_2\right) \\
&\quad \times \mathcal{N}(x_{1:2}, \overline{x}^{i,\widetilde{a}^i}_{k+1|k}(2), P^{i,\widetilde{a}^i}_{k+1|k}(2))dx_{1:2} \qquad (112)\\
&= p^D \beta^{i,a^i}_{k+1|k+1}(2)\mathcal{N}\left(z_{1:2}; \overline{z}^{i,a^i}, S_{i,a^i}\right), \qquad (113)
\end{aligned}$$

where

$$\overline{z}^{i,a^i} = H_{3,3}\overline{x}^{i,\widetilde{a}^i}_{k+1|k}(2) \qquad (114)$$

$$S_{i,a^i} = H_{3,3}P^{i,\widetilde{a}^i}_{k+1|k}(2)H^T_{3,3} + R_2, \qquad (115)$$

with $H_{3,3} = I_2 \otimes H$ and $R_2 = I_2 \otimes R$. The expression for the weight (66) follows directly from (113). Based on (25), the Kalman update gives the parameters for the updated single-trajectory density of the form (40).

3) Measurement detected only at time step $k+1$: If $Z^j = (k+1, z_1) \in M^2$, the measurement model takes the form of (9b) for $X \in T^3$, while it is zero for $X \in T^1$. Therefore, (105) yields a non-zero term corresponding to $l = 2$ in (40)

$$\begin{aligned}
&\langle\, p^{i,\widetilde{a}^i}_{k+1|k}, l\left(Z^j_{k+1}|\cdot\right) p^D \rangle \\
&= p^D \beta^{i,a^i}_{k+1|k}(2)\gamma \\
&\quad \times \int_{\mathbb{R}^{2n_x}} h_{2,3}(z_1|x_{1:2})\mathcal{N}(x_{1:2}, \overline{x}^{i,\widetilde{a}^i}_{k+1|k}(2), P^{i,\widetilde{a}^i}_{k+1|k}(2))dx_{1:2} \qquad (116)\\
&= p^D \beta^{i,a^i}_{k+1|k}(2)\gamma \int_{\mathbb{R}^{2n_x}} \mathcal{N}\left(z_1; H_{2,3}x_{1:2}, R_1\right) \\
&\quad \times \mathcal{N}(x_{1:2}, \overline{x}^{i,\widetilde{a}^i}_{k+1|k}(2), P^{i,\widetilde{a}^i}_{k+1|k}(2))dx_{1:2} \qquad (117)\\
&= p^D \beta^{i,a^i}_{k+1|k+1}(2)\mathcal{N}\left(z_1; \overline{z}^{i,a^i}, S_{i,a^i}\right), \qquad (118)
\end{aligned}$$

where

$$\overline{z}^{i,a^i} = H_{2,3}\overline{x}^{i,\widetilde{a}^i}_{k+1|k}(2) \tag{119}$$

$$S_{i,a^i} = H_{2,3}P^{i,\widetilde{a}^i}_{k+1|k}(2)H^T_{2,3} + R_2, \tag{120}$$

with $H_{2,3} = [0,1] \otimes H$ and $R_2 = I_2 \otimes R$. The expression for the weight (66) follows directly from (113). Based on (25), the Kalman update gives the parameters for the updated single-trajectory density of the form (40).

B. New Bernoulli component

According to Lemma 4, the predicted intensity is a Gaussian mixture intensity comprising two different kinds of components, denoted as b and p in (43). Based on Lemma 2, the detection hypothesis of a new Bernoulli component $f^{i,a^i}_{k+1|k+1}(\cdot)$, $i \in \{n_{k+1|k}+j\}$, $j \in \{1,\ldots,m_{k+1}\}$, initiated by the trajectory measurement $Z^j = (t, z_{1:\nu}) \in M^\mu$is computed by evaluating the inner product $\left\langle \lambda_{k+1|k}, l\left(Z^j|\cdot\right) p^D \right\rangle$.

For the q_b-th component of the mixture b in (43), the measurement model is non-zero only if $Z^j = (k+1, z_1) \in M^2$ and takes the form of (9e). Therefore,

$$\begin{aligned} v^{b,q_b} &= \left\langle \lambda_{k+1|k}, l\left(Z^j|\cdot\right) p^D \right\rangle \\ &= w^{b,q_b}_{k+1|k} p^D \int_{\mathbb{R}^{n_x}} h_{2,2}(z_1|x_1)\mathcal{N}(x_1, \overline{x}^{b,q_b}_{k+1|k}, P^{b,q_b}_{k+1|k})dx_1 \end{aligned} \tag{121}$$

$$\begin{aligned} &= w^{b,q_b}_{k+1|k} p^D \\ &\quad \times \int_{\mathbb{R}^{n_x}} \mathcal{N}(z_1, Hx_1, R_1)\mathcal{N}(x_1, \overline{x}^{b,q_b}_{k+1|k}, P^{b,q_b}_{k+1|k})dx_1 \end{aligned} \tag{122}$$

$$= w^{b,q_b}_{k+1|k} p^D \mathcal{N}(z_1, H\overline{x}^{b,q_b}_{k+1|k}, S_{b,q_b}), \tag{123}$$

where $S_{b,q_b} = HP^{b,q_b}_{k+1|k}H^T + R$. For the q_p-th component of the mixture p in (43), the measurement model is in the forms of (9c)-(9b), and the correspondent inner product v^{p,q_p} can be computed similarly to (108)-(118).

Once the inner products are computed, (82) and (83) follow directly from (26) and (27). Finally, from (28), the single-trajectory density of the new Bernoulli component is a Gaussian mixture, where each component results from a Kalman update based on (123) or (80), similar to the Bernoulli competent updates in Sec. A-A. In this paper, we propose to use a Gaussian approximation of the resulting mixture (84).

APPENDIX B
HYPOTHESIS-COUNT ANALYSIS

In this appendix, we present a hypothesis-count analysis of the TM-PMBM/TM-PMB and PMBM/PMB filters to justify the computational times in Tab. I. Fig. 9 shows the average number of single-target hypotheses and global hypotheses in the filters at each time step (or two-time step window), for the simulations based on Scenario 1 in Sec. V-B. Apart from the case with $N_w = 2$, Fig. 9 shows that the TM-PMBM/TM-PMB filters operate with fewer single-target and global hypotheses than the standard PMBM/PMB filters.

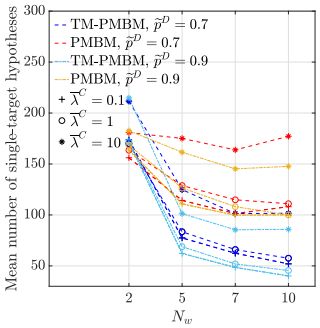

(a) Mean number of single-target hypotheses per time step, averaged over 30 MC runs, for the TM-PMBM and PMBM filters.

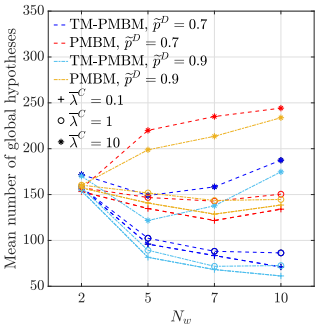

(b) Mean number of global hypotheses per time step, averaged over 30 MC runs, for the TM-PMBM and PMBM filters.

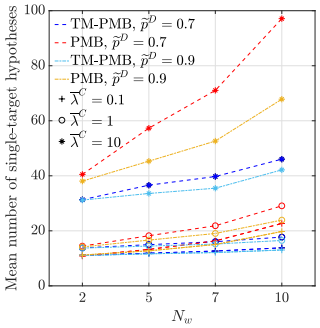

(c) Mean number of single-target hypotheses per time step, averaged over 30 MC runs, for the TM-PMB and PMB filters.

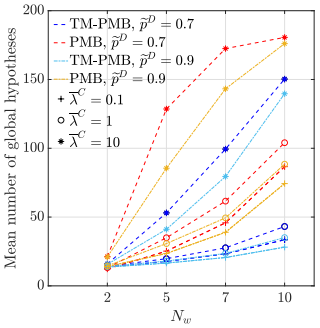

(d) Mean number of global hypotheses per time step, averaged over 30 MC runs, for the TM-PMB and PMB filters.

Figure 9: Hypothesis-count analysis for simulations in Scenario 1.